EFFECT OF DIE EXIT STRESS STATE, DEBORAH NUMBER, UNIAXIAL AND PLANAR EXTENSIONAL RHEOLOGY ON THE NECK-IN PHENOMENON IN POLYMERIC FLAT FILM PRODUCTION

Tomas Barborik, Martin Zatloukal*

Polymer Centre, Faculty of Technology, Tomas Bata University in Zlin,

Vavreckova 275, 760 01 Zlin, Czech Republic

Keywords: Flat film production, polymer melt, rheology, neck-in phenomenon, Deborah number, second to first normal stress difference ratio, uniaxial extensional viscosity, planar extensional viscosity.

*Corresponding author: mzatloukal@utb.cz

1 ABSTRACT

In this work, effect of the second to first normal stress difference ratio at the die exit, $-N_2/N_1$, uniaxial extensional strain hardening, $\frac{\eta_{E,U,max}}{3\eta_0}$, planar-to-uniaxial extensional viscosity ratio, $\frac{\eta_{E,P}}{\eta_{E,U}}$, and Deborah number, *De*, has been investigated via viscoelastic isothermal modeling utilizing 1D membrane model and a single-mode modified Leonov model as the constitutive equation. Based on the performed parametric study, it was found that there exists a threshold value for *De* and $\frac{\eta_{E,U,max}}{3\eta_0}$, above which, the neck-in starts to be strongly dependent on $-N_2/N_1$. It was found that such critical *De* decreases if $-N_2/N_1$, $\frac{\eta_{E,U,max}}{3\eta_0}$ increases and/or $\frac{\eta_{E,P}}{\eta_{E,U}}$ decreases. Numerical solutions of the utilized model were successfully approximated by a dimensionless analytical equation relating the normalized maximum attainable neck-in with $\frac{\eta_{E,U,max}}{3\eta_0}$, $\frac{\eta_{E,P}}{\eta_{E,U}}$, $-N_2/N_1$ and *De*. Suggested equation was tested by using literature experimental data considering that $-N_2/N_1$ depends on die exit shear rate, temperature and utilized constitutive model parameters for given polymer melt. It was found that approximate model predictions are in a very good agreement with the corresponding experimental data for low as well as very high Deborah numbers, at which neck-in strongly depends on $-N_2/N_1$. It is believed that the obtained knowledge together with the suggested simple model can be used for optimization of the extrusion die design (influencing flow history and thus die exit stress state), molecular architecture of polymer melts and processing conditions to suppress neck-in phenomenon in production of very thin polymeric flat films.

2 INTRODUCTION

The extrusion film casting technology is an industrially important process that has a firm position on the market due to its capability to produce high quality thin polymeric films at high production rates. Those films can be used in different applications such as wrapping materials, barriers reducing permeability for air and vapor, or as a separator membrane for rechargeable batteries in mobile devices and electric vehicles.

In this technology, the polymer melt is extruded through a slit die to form a thick sheet that is subsequently intensively stretched in the axial direction, hauled off and quenched by a rotating drum stabilizing the film dimensions. [1,2] (Fig. 1). Except of an initial swelling, the thickness of the film decreases monotonically due to high Draw ratio (the haul off speed divided by the die exit velocity). In such a case, film width is gradually reduced toward the stretching/cooling roll, which is called neck-in phenomenon.

Aside from that, the interrelated defect of edge-beads promotes the lateral portion of the film to being substantially thicker than its central part (Fig. 2). While the first phenomenon affects a production rate, the second calls for a post-production trimming since solely central portion of the film is uniform in thickness. Understanding the relationship between material parameters and processing conditions including the flow in the die might be the way to effectively control the extent of neck-in and edge-beading as even a small reduction of these defects may bring increased efficiency considering high production rates in this manufacturing process.

Scientific investigation of the extrusion film casting process has been addressed in many works dealing with both a steady and transient approaches to the problem. Initial studies were dedicated to an investigation of the hydrodynamic instability observed during the production of fibers called draw resonance [3–5] and then expanded for films in [6] where the numerical

modeling for film casting using the one-dimensional isothermal model of Newtonian fluid was utilized for the first time. Other authors followed and employed different constitutive equations for power-law [7], and viscoelastic fluids using modified convected-Maxwell [8] and modified Giesekus model [9,10]. Due to the assumed kinematics for the free surface flow at the drawing zone, the model could not capture edge-bead defect and contraction in film width.

First efforts to overcome this limitation and to accommodate ability to predict neck-in were made for a Newtonian fluid at isothermal [11] and non-isothermal conditions [12–14]. Lately, improved isothermal two-dimensional membrane model having the capability to capture the development of edge-beads under the stationary conditions was released; isothermal Newtonian [15] and viscoelastic Maxwell and Giesekus fluid [16], and models that take thermal effects into account for Newtonian [17] and viscoelastic Larson fluid [18]. In the meantime, simplified one-dimensional membrane approach based on a supplementary kinematic hypothesis, that originally brought for a float glass stretching [19], was proposed [20] and an extended isothermal study on the influence of processing conditions on the film geometry for casting of Newtonian and Maxwell fluids was carried out. Owing to the assumed flow kinematics, this model could cover a film width reduction but was not able to predict edge-beading. This restriction was removed in the succeeding work [21]. A cutting-edge three-dimensional model for extrusion film casting simulation was further established for a steady Newtonian isothermal [22] and non-isothermal [23] fluid.

A specific attention was given at certain aspects of the process. The effect of thermal conditions including crystallization [24–31] as well as influence of macromolecular architecture on the extent of neck-in [32–36] was put under research abundantly. More recently, a sequence of articles based on the one-dimensional membrane model [20] have been published dealing with both experimental and theoretical investigation of the effects of

long chain branching and molecular weight distribution on the neck-in [37–39] (XPP and RP-s), and discussing the role of individual viscoelastic relaxation modes of a polymer melt [40] (UCM and PTT). In the latest works of this series [41] and [42], the evaluation of a draw resonance onset with model based on PTT constitutive equation and neck-in degree simulation using two-dimensional model with UCM constitutive equation [33] was addressed, respectively.

The key findings with respect to formation of edge-beads and neck-in were postulated in [43], where the authors pointed out that the deformation flow in the drawing zone comprises of two related regions and the extent of these phenomena is determined by the interplay between them through an edge stress effect, as illustrated in Fig. 3. Planar extensional deformation is experienced in a central region of the film and uniaxial extensional one in lateral parts. This led to that some authors have chosen an approach relating the level of the observed necking in terms of rheological parameters and reported that a degree of neck-in phenomenon may be depressed by a strain hardening in uniaxial extensional viscosity [16,18,44,45]. This conception was slightly more developed in the succeeding studies where the neck-in extent was connected with the ratio of planar viscosities in axial and transverse directions [33], and recently, with the ratio of planar to uniaxial extensional viscosity [46–48] reflecting the flow kinematics in a drawing zone according to [43].

In order to resolve the system of model equations proposed in above mentioned studies, it is necessary to have fully satisfied boundary conditions. This is problematic for the cases, in which viscoelastic constitutive equations are used because an additional boundary stress condition at the die exit must be specified. Its value should be determined by both, a polymer flow in the upstream and downstream region (i.e. depending on an in-die complex flow) and a extensional flow in the drawing zone [49]. Among the various authors, one can find following strategies on how to deal with this problem. First, all stress components are set to

zero considering entire stress relaxation due to the die swell phenomenon ([16,17,50] and [51]). Second, at least one stress component is given by a Newtonian solution for downstream side independently on the utilized type of constitutive equation [18], [20,21], [39], [41], [52] and [53]. Third, two extra stress components are adjusted manually without more reasoning [37,38,40]. Fourth, the die exit stress state is given by axial upstream extra stress component [8], thickness to axial extra stress component ratio for upstream/downstream side [9,54] or by second to first normal stress difference ratio, $-N_2/N_1$, calculated from upstream side [55] by using viscoelastic constitutive equation. It has been found that if Deborah number is low (0.00161 [49]; 0.07 [20,21]; 0.1 [9,56]), the choice of the initial stress conditions at the die have only a little influence on the steady-state calculations. However, at high Deborah numbers (*De = 0.124* [8]) it seems that the die exit stress state, which can be influenced for example by extrusion die design [57] starts to have a significant impact on the neck-in phenomenon.

In this article, as a part of circumstantial set of our studies on the free-surface flow instabilities [58–60], the effect of die exit stress state, extensional rheology and Deborah number on the neck-in phenomenon is systematically investigated via viscoelastic isothermal modeling (utilizing 1D membrane model coupled with a single-mode modified Leonov model) and obtained results are compared with suitable literature experimental data.

3 MATHEMATICAL MODELING

3.1 Modified Leonov model

The utilized modified Leonov model is based on heuristic thermodynamic arguments resulting from the theory of rubber elasticity [61–66]. In this constitutive equation, a fading

memory of the melt is determined through an irreversible dissipation process driven by the dissipation term, *b*. From mathematical viewpoint, it is relating the stress and elastic strain stored in the material as:

$$\underline{\underline{\tau}} = 2\left(\underline{\underline{c}} \cdot \frac{\partial W}{\partial I_{1,c}} - \underline{\underline{c}}^{-1} \cdot \frac{\partial W}{\partial I_{2,c}} \right) \tag{1}$$

where $\underline{\underline{\tau}}$ is the stress, and *W*, the elastic potential, which depends on the invariants $I_{1,c}$ and $I_{2,c}$ of the recoverable Finger tensor $\underline{\underline{c}}$,

$$W = \frac{3G}{2(n+1)} \left\{ [1-\beta] \cdot \left[\left(\frac{I_{1,c}}{3} \right)^{n+1} - 1 \right] + \beta \left[\left(\frac{I_{2,c}}{3} \right)^{n+1} - 1 \right] \right\} \tag{2}$$

where *G* denotes linear Hookean elastic modulus, β and *n* are numerical parameters. Leonov assumed that the dissipative process acts to produce an irreversible rate of strain e_p

$$\underline{\underline{e}}_p = b\left[\underline{\underline{c}} - \frac{I_{1,c}}{3} \underline{\underline{\delta}} \right] - b\left[\underline{\underline{c}}^{-1} - \frac{I_{2,c}}{3} \underline{\underline{\delta}} \right] \tag{3}$$

which spontaneously reduces the rate of elastic strain accumulation. Here, $\underline{\underline{\delta}}$ is the unit tensor and *b* stands for dissipation function defined by Eq. 5. This elastic strain $\underline{\underline{c}}$ is related to the deformation rate tensor $\underline{\underline{D}}$ as follows

$$\overset{\circ}{\underline{\underline{c}}} - \underline{\underline{c}} \cdot \underline{\underline{D}} - \underline{\underline{D}} \cdot \underline{\underline{c}} + 2\underline{\underline{c}} \cdot \underline{\underline{e}}_p = 0 \tag{4}$$

where $\overset{\circ}{\underline{\underline{c}}}$ is the Jaumann (corotational) time derivative of the recoverable Finger strain tensor. In this work, the Mooney potential (i.e. *n = 0* in Eq. 2), and the dissipation function *b* proposed in [67] (see Eq. 5) have been employed.

$$b(I_{1,c}) = \frac{1}{4\lambda} \left\{ \exp\left[-\xi \sqrt{I_{1,c} - 3} \right] + \frac{\sinh\left[\nu (I_{1,c} - 3) \right]}{\nu (I_{1,c} - 3) + 1} \right\} \tag{5}$$

Here, ξ and ν are adjustable model parameters.

3.2 Extrusion film casting model

In this study, one-dimensional membrane model [20] was used to simulate the drawing process of a molten film in the post extrusion die area. The model is capable to predict film width shrinkage despite its dimensionality due to the applied flow kinematics assumptions [19] allowing principal velocity variation along the axial direction (Fig. 1) as follows

$$\begin{aligned} u &= u(x) \\ v &= v(x, y) = yf(x) \\ w &= w(x, z) = zg(x) \end{aligned} \tag{6}$$

Here *u*, *v* and *w* stands for the velocities in axial, transversal and thickness direction, respectively. The membrane model comprises of equations for continuity and momentum conservation that are simultaneously solved with viscoelastic single-mode modified Leonov model as the constitutive equation. The main model equations are summarized below in dimensionless form utilizing dimensionless quantities provided in Table. 1 (having a similar form as in [20] to keep consistency with the open literature).

In this table, τ_{ii} is the *ii* component of the extra stress tensor; *F* and *E*, drawing and dimensionless drawing force exerted onto film; *DR*, draw ratio; *De*, Deborah number; λ, relaxation time; *G*, elastic modulus; *A*, aspect ratio; *X* and *x*, drawing distance and actual axial position and *L*, *e*, *u*, are half-width, half-thickness and axial velocity of the film. The zero subscript and overbar sign denotes initial and dimensionless corresponding quantity, respectively.

Mass conservation equation is given by the following equation

$$\bar{e}\bar{L}\bar{u} = 1 \tag{7}$$

Considering the membrane approximation for a thin film in the presence of a constant drawing force, the momentum conservation equation yields

$$\left(\bar{\tau}_{xx} - \bar{\tau}_{zz}\right) - \bar{u} = 0 \tag{8}$$

The kinematic free-surface and stress-free surface boundary condition allows determination of unknown functions appearing in Eq. 6. (i.e. *f(x)* and *g(x)*) and the film width-stress relationship at given dimensionless axial position, $\bar{x}$, Eq. 9, respectively.

$$\frac{d\bar{L}}{d\bar{x}} = -A\sqrt{\frac{\bar{\tau}_{yy} - \bar{\tau}_{zz}}{\bar{\tau}_{xx} - \bar{\tau}_{zz}}} \tag{9}$$

Differentiating Eqs. 7 and 8 with respect to $\bar{x}$ variable and after algebraic rearrangement, the derivative of the dimensionless film half-thickness with respect to $\bar{x}$ leads to

$$\frac{d\bar{e}}{d\bar{x}} = -\left(\frac{1}{\bar{L}}\frac{d\bar{L}}{d\bar{x}} + \frac{1}{\bar{u}}\frac{d\bar{u}}{d\bar{x}}\right)\bar{e} \tag{10}$$

Utilization of Mooney potential in the modified Leonov model constitutive equation (i.e. when $n = 0$ and $\beta \neq 0$ in Eq. 2), the relationship between the dimensionless stress and recoverable strain takes the following form

$$\bar{\tau}_{ii} = \frac{E}{De}c_{ii} - \frac{E}{De}c_{ii}\cdot\beta - \frac{E}{De}c_{ii}^{-1}\cdot\beta \tag{11}$$

In combination of the membrane model and constitutive equation, the derivative of diagonal components of the recoverable strain tensor, c_{ii}, with respect to $\bar{x}$ are given in form

$$\frac{dc_{xx}}{d\bar{x}} = 2c_{xx}\frac{1}{\bar{u}}\frac{d\bar{u}}{d\bar{x}} - \frac{2\bar{b}}{\bar{u}}Z_x \tag{12}$$

$$\frac{dc_{yy}}{d\bar{x}} = 2c_{yy}\frac{1}{\bar{L}}\frac{d\bar{L}}{d\bar{x}} - \frac{2\bar{b}}{\bar{u}}Z_y \tag{13}$$

$$\frac{dc_{zz}}{d\bar{x}} = 2c_{zz}\frac{1}{\bar{e}}\frac{d\bar{e}}{d\bar{x}} - \frac{2\bar{b}}{\bar{u}}Z_z \tag{14}$$

where the dimensionless dissipation function, $\bar{b}$, and Z_i are defined as

$$\bar{b}\left(I_{1,c}\right)=\frac{1}{4De}\left\{\exp\left[-\xi\sqrt{I_{1,c}-3}\right]+\frac{\sinh\left[\nu\left(I_{1,c}-3\right)\right]}{\nu\left(I_{1,c}-3\right)+1}\right\} \tag{15}$$

$$Z_i = c_{ii}\left[c_{ii}-c_{ii}^{-1}+\frac{1}{3}\left(c_{xx}^{-1}+c_{yy}^{-1}+c_{zz}^{-1}-c_{xx}-c_{yy}-c_{zz}\right)\right] \tag{16}$$

Combination of Eqs. 7, 8 and 11 leads to the dimensionless streamwise deformation rate, which takes the following form

$$\frac{d\bar{u}}{d\bar{x}}=\frac{\bar{b}\left[\beta\left(Z_x-Z_z\right)-Z_x+Z_z\right]+\bar{b}\beta\left(\frac{1}{c_{zz}^2}Z_z-\frac{1}{c_{xx}^2}Z_x\right)+\frac{\bar{u}}{\bar{L}}\frac{d\bar{L}}{d\bar{x}}\left(c_{zz}\left(1-\beta\right)+\frac{\beta}{c_{zz}}\right)}{\beta\left(c_{xx}+c_{zz}\right)-c_{xx}-c_{zz}-\frac{\beta}{c_{xx}}\left(\frac{c_{zz}+c_{xx}}{c_{zz}}\right)+\frac{De\bar{u}}{2E}} \tag{17}$$

Eqs. 9, 10, 12, 13, 14 and 17 represent the final set of equations for isothermal viscoelastic 1D membrane model utilized in this work. More detailed derivation of the model is provided in our previous work [55]. Note that due to a geometrical symmetry of the film, only 1/4th of the film cross-section can be used in the calculation as showed in [68].

3.3 Boundary Conditions

In order to solve the model equations, boundary conditions for downstream, Eq. 18, and upstream region, Eq. 19, have to be provided.

$$\bar{u}\left(X\right)=DR \tag{18}$$

$$\begin{gathered}\bar{u}\left(0\right)=1 \qquad \bar{e}\left(0\right)=1 \qquad \bar{L}\left(0\right)=1 \\ \bar{\tau}_{xx}\left(0\right) \qquad \bar{\tau}_{yy}\left(0\right) \qquad \bar{\tau}_{zz}\left(0\right)\end{gathered} \tag{19}$$

At the downstream region, draw ratio is prescribed as the desired value that is satisfied by a priori unknown magnitude of the drawing force. Upstream area (i.e. extrusion die exit region) is defined by the known average melt speed and die dimensions (gap size and width) whereas diagonal components of the extra stress tensor $\bar{\tau}_{xx}$, $\bar{\tau}_{yy}$ and $\bar{\tau}_{zz}$ have to be calculated

via Eq. 11 utilizing c_{xx}, c_{yy} and c_{zz} components of the recoverable strain tensor satisfying the following set of equations:

$$\frac{E}{De}\left[\left(c_{xx}-c_{zz}\right)\left(1-\beta\right)+\beta\left(c_{zz}^{-1}-c_{xx}^{-1}\right)\right]-1=0 \tag{20}$$

$$c_{xx}c_{yy}c_{zz}=1 \tag{21}$$

$$-\frac{N_2}{N_1}=\frac{E\left[c_{zz}-c_{yy}+\beta\left(c_{yy}+c_{yy}^{-1}-c_{zz}-c_{zz}^{-1}\right)\right]}{De\bar{u}} \tag{22}$$

Eq. 20 arises from the momentum conservation equation (Eq. 8), Eq. 21 from the melt incompressibility assumption and Eq. 23 characterizes the polymer melt stress state at the die exit region as the ratio of the secondary to primary normal stress difference, $-N_2/N_1$. This ratio is calculated from the fully-developed slit flow at the extrusion die exit as follows

$$-\frac{N_2}{N_1}=-\frac{\bar{\tau}_{zz}(0)-\bar{\tau}_{yy}(0)}{\bar{\tau}_{xx}(0)-\bar{\tau}_{zz}(0)} \tag{23}$$

3.4 Numerical Scheme

The entire set of the first-order ordinary differential equations, which comprises from equations for film half-width (Eq. 9), half-thickness (Eq. 10), velocity (Eq. 17), components of the recoverable elastic strain tensor (Eqs. 12-14) and boundary conditions (Eqs. 20-23), was solved by 4th order Runge-Kutta method implementing adaptive step-size control. At the beginning, take-up force was guessed and consequently increased or decreased for every following iteration until the given draw ratio was achieved. Solver was developed in the C++ programming language and coupled with GNUPLOT plotting software for automatic graph generation. Typical computational time for one calculation of prescribed *DR* was about 2 minutes on the PC with the following hardware parameters: CPU: Intel Core 2 Quad

Q9650 (3.00 GHz), RAM: 8 GB DDR2, GPU: Sapphire Radeon HD 3870, SSD: Crucial 256 GB.

4 RESULTS AND DISCUSSION

4.1 Theoretical analysis of neck-in phenomenon

4.1.1 The role of extensional rheology, Deborah number and $-N_2/N_1$ ratio at the die exit

In order to understand the role of extensional rheology, Deborah number and die exit stress state on the maximum attainable neck-in, 3 groups of virtual materials having three different levels of uniaxial strain hardening defined by Eq. 24 were used.

$$\frac{\eta_{E,U,max}}{3\eta_0} \tag{24}$$

Here, $\eta_{E,P,max}$ is the maximum steady uniaxial extensional viscosity and η_0 stands for the Newtonian viscosity. In each group, 5 virtual materials were generated having the same level of uniaxial extensional strain hardening (1.3, 3.4 and 7.1) but different level of planar extensional strain hardening (1.10-1.53, 2.9-4.2 and 6.2-7.9) and the zero-shear rate second to first normal stress difference ratio (0.3-0.6) defined by Eq. 25 and Eq. 26, respectively.

$$\frac{\eta_{E,P,max}}{4\eta_0} \tag{25}$$

$$\lim_{\dot{\gamma}\to 0}\left(-\frac{N_2}{N_1}\right) \tag{26}$$

Here, $\eta_{E,P,max}$ is the maximum steady planar extensional viscosity, $\dot{\gamma}$ is the shear rate, N_1 and N_2 is the first and second normal stress difference at the die exit defined (for the post-die coordinate system depicted in Fig. 1) as follows

$$N_1 = \tau_{xx} - \tau_{zz} \tag{27}$$

$$N_2 = \tau_{zz} - \tau_{yy} \tag{28}$$

Modified Leonov model parameters together with corresponding $\frac{\eta_{E,U,max}}{3\eta_0}$, $\frac{\eta_{E,P,max}}{4\eta_0}$ and $\lim_{\dot{\gamma}\to 0}\left(-\frac{N_2}{N_1}\right)$ values are provided in Tab. 2 for the 15 utilized virtual polymer melts.

Deborah number was varied from 0.01 to 0.3 in the film casting model for all 15 virtual polymer melts changing the $-N_2/N_1$ ratio from 0.001 to 2. For each simulation case, the draw ratio was adjusted high enough (typically equal to 40) in order to reach a maximum and draw ratio independent neck-in value, *NI*. Note that the neck-in is defined as $L_0 - L(X)$, see Figures 1-2. The maximum neck-in value was consequently normalized by the take-up length, *X*, as follows.

$$NI^* = \frac{NI}{X} \tag{29}$$

In order to visualize obtained trend, calculated maximum neck-in value NI^* as a function of the square root of planar to uniaxial extensional viscosity ratio, $\sqrt{\frac{\eta_{E,P}}{\eta_{E,U}}}$, is provided in Figure 4 for three selected Deborah numbers (0.01, 0.05 and 0.3), two uniaxial extensional strain hardening values (1.3 and 7.1) and two $-N_2/N_1$ ratios (0.001 and 1). It is visible that firstly, an increase in the Deborah number and $-N_2/N_1$ ratio increases both, the normalized neck-in as well as its sensitivity to $\sqrt{\frac{\eta_{E,P}}{\eta_{E,U}}}$ and secondly, there exists threshold value for Deborah number and uniaxial extensional strain hardening, above which, the neck-in phenomenon starts to be dependent on the die exit stress state. Critical Deborah number was calculated for given $-N_2/N_1$ ratio, above which, a considerable deviation (more than 5 %) in the neck-in value starts to occur. Here, the neck-in at $-N_2/N_1 = 0.001$ was taken as the

reference. The effect of $-N_2/N_1$ ratio and uniaxial extensional strain hardening, $\frac{\eta_{E,U,max}}{3\eta_0}$, (keeping the ratio of planar to uniaxial extensional strain hardening value, $\frac{\eta_{E,P,max}}{4\eta_0} / \frac{\eta_{E,U,max}}{3\eta_0}$, the same, equal to one) on the critical Deborah number is provided in Figure 5a utilizing three virtual melts (namely Melt4_Low, Melt4_Middle, Melt4_High, see Table 2). In this image, area below the lines represents conditions, at which the $-N_2/N_1$ ratio has practically no effect (namely lower than 5 %) on the normalized maximum attainable neck-in, whereas above these lines, the $-N_2/N_1$ starts to have a considerable effect (more than 5 %) on the neck-in phenomenon. As it can be seen, firstly, the critical Deborah number decreases with increased $-N_2/N_1$ and secondly, an increase in $\frac{\eta_{E,U,max}}{3\eta_0}$ decreases the critical Deborah number for given value of $-N_2/N_1$. For example, adjusting $-N_2/N_1 = 0.2$ and changing $\frac{\eta_{E,U,max}}{3\eta_0}$ to 1.3, 3.4 and 7.1 yields critical Deborah number equal to 0.158, 0.073 and 0.042, respectively.

The effect of $\frac{\eta_{E,P,max}}{4\eta_0} / \frac{\eta_{E,U,max}}{3\eta_0}$ (changing from 0.85 to 1.24) and $\frac{\eta_{E,U,max}}{3\eta_0}$ (changing from 1.3 to 7.1) is visualized in Figure 5b)-5d). Here, it is visible that increase in $\frac{\eta_{E,P,max}}{4\eta_0} / \frac{\eta_{E,U,max}}{3\eta_0}$ increases the critical Deborah number for given $\frac{\eta_{E,U,max}}{3\eta_0}$ and $-N_2/N_1$ values. The effect was found to be more dominant for lower $-N_2/N_1$ and higher $\frac{\eta_{E,U,max}}{3\eta_0}$.

From these results, it can be concluded that die exit stress state, characterized via $-N_2/N_1$ ratio, has to be defined properly in order to predict the normalized maximum attainable

neck-in correctly, especially at high Deborah numbers for polymer melts with high $\frac{\eta_{E,U,max}}{3\eta_0}$ and low $\frac{\eta_{E,P,max}}{4\eta_0} / \frac{\eta_{E,U,max}}{3\eta_0}$.

Note that $-N_2/N_1$ can be viewed as the variable, which is inversely proportional to the melt planar pre-stretching at the die exit. Thus the basic trend depicted in Figure 5 can be physically interpreted as follows. If the level of planar pre-stretching decreases, its effect on the maximum attainable neck-in starts to occur at lower Deborah numbers.

*4.1.2 Analytical approximation for NI**

All numerical predictions of the utilized viscoelastic film casting model for normalized neck-in value NI^* vs. square root of planar to uniaxial extensional viscosity ratio $\sqrt{\frac{\eta_{E,P}}{\eta_{E,U}}}$ and considering different Deborah numbers (0.01-0.30), uniaxial extensional strain hardening (1.3-7.1) and $-N_2/N_1$ ratios (0.001-2) is provided in Figures 6-9 as the symbols. In our previous work [55], it has been found that numerical solution for NI^* can be approximated by Eq. 30, if the role of $-N_2/N_1$ on the neck-in phenomenon is neglected.

$$NI^* = \frac{1}{\sqrt[10]{\frac{\eta_{E,U,max}}{3\eta_0}}} \left\{ A_1 \left[1 - \exp\left(-\alpha_1 De^{\varphi_1}\right)\right] \left(\sqrt{\frac{\eta_{E,P}}{\eta_{E,U}}} - 1 \right) + A_2 \left[1 - \exp\left(-\alpha_2 De^{\varphi_2}\right)\right] \right\} \qquad (30)$$

where A_1, α_1, φ_1, A_2, α_2, φ_2 are model constants. In order to include the effect of $-N_2/N_1$ ratio on NI^*, we have modified Eq. 30 for NI^* introducing $-N_2/N_1$ ratio via specific type of δ function and utilizing five additional constants θ, ψ_1, ψ_2, ψ_3 and ψ_4. Suggested modified equation for the NI^* is given by Eq. 31.

$$NI^{*}=\frac{1}{\sqrt[\theta]{\frac{\eta_{E,U,max}}{3\eta_0}}}\left\{A_1\left[1-\exp\left(-\alpha_1 De^{\varphi_1}\right)\right]\left(\sqrt{\frac{\eta_{E,P}}{\eta_{E,U}}}-1\right)+\delta A_2\left[1-\exp\left(-\alpha_2 De^{\varphi_2}\right)\right]\right\} \tag{31}$$

where

$$\delta=1+\psi_1\arctan\left(\psi_2\frac{N_2}{N_1}\right)\arctan\left(\psi_3\frac{\eta_{E,U,max}}{3\eta_0}\tanh\left(\psi_4 De\right)\right) \tag{32}$$

and Deborah number, *De*, is given by $De=\frac{\lambda u_0}{X}$.

Eq. 31 was used to fit all numerical neck-in predictions for all considered planar to uniaxial extensional viscosity ratios, Deborah numbers, uniaxial extensional strain hardenings and $-N_2/N_1$ ratios, which are depicted in Figures 6-9. All identified constants of Eq. 31 together with Root Mean Square Error, *RMSE*, which characterizes the overall fitting error (see definition bellow), are provided in Table 3.

$$RMSE=\sqrt{\frac{1}{n_s}\sum_{j=1}^{n_s}\left[y_j-\hat{y}_j\right]^2} \tag{33}$$

where n_s is the number of points whereas y_j and $\hat{y}_j$ represent given and predicted points, respectively. As it can be seen, the simple approximate solution model (Eq. 31) has very high capability to represent NI^* predictions of the utilized 1D viscoelastic membrane model very well.

4.1.3 Behavior of analytical approximation for NI^* at high Deborah numbers

For very high Deborah numbers, Eq. 31 for NI^* simplifies to

$$\lim_{De\to\infty} NI^{*}=\frac{1}{\sqrt[\theta]{\frac{\eta_{E,U,max}}{3\eta_0}}}\left\{\begin{array}{l}A_1\left(\sqrt{\frac{\eta_{E,P}}{\eta_{E,U}}}-1\right)+\\ A_2\left[1+\psi_1\arctan\left(\psi_2\frac{N_2}{N_1}\right)\arctan\left(\psi_3\frac{\eta_{E,U,max}}{3\eta_0}\right)\right]\end{array}\right\} \tag{34}$$

Considering that A_1 and A_2 are identical during a fitting procedure utilizing Eq. 31, the change in *RMSE* is very small (from 0.020888 to 0.023903), which justifies to use this assumption to further simplify Eq. 34 as follows

$$\lim_{De\to\infty} NI^{*} = \frac{A_1}{\sqrt[\theta]{\frac{\eta_{E,U,max}}{3\eta_0}}}\left[\sqrt{\frac{\eta_{E,P}}{\eta_{E,U}}} + \psi_1 \arctan\left(\psi_2 \frac{N_2}{N_1}\right)\arctan\left(\psi_3 \frac{\eta_{E,U,max}}{3\eta_0}\right)\right] \qquad (35)$$

where $A_1 = 0.493$, $\theta = 7.65$, $\psi_1 = 0.985$, $\psi_2 = 0.812$, $\psi_3 = 0.524$.

As it can be deduced from Eq. 35, a limiting value of NI^{*} is a linear function of $\sqrt{\frac{\eta_{E,P}}{\eta_{E,U}}}$ with a slope of $\frac{0.493}{\sqrt[7.65]{\frac{\eta_{E,U,max}}{3\eta_0}}}$ and non-zero limiting NI^{*} intercept value depending on $-N_2/N_1$ as well as $\frac{\eta_{E,U,max}}{3\eta_0}$.

4.2 Analytical approximation for NI^{*} vs. experimental data

The approximate solution given by Eq. 31, utilizing constants provided in Table 3, was validated for 5 different polyethylenes with basic characteristics summarized in Table 4.

In the first step, deformation rate dependent 'steady state' uniaxial extensional viscosity data (taken from the transient viscosity data peaks for given deformation rates, [60] and [69]) were fitted by the modified Leonov model (Eqs. 1-5) to identify its parameters, which are summarized in Table 5. It is important to note that in the case of LDPE 170A sample, even if it was possible to fit experimental points by 5 different sets of Leonov model parameters with a practically identical error (because number of experimental points was very low, see Figure 10a), corresponding model predictions for $\frac{\eta_{E,P}}{\eta_{E,U}}$ and $-N_2/N_1$ were different (see Figure 10b-10c). This has a strong impact on the viscoelastic 1D membrane model

predictions for dimensionless final film half-width vs. draw ratio, especially, for high Deborah numbers, at which $-N_2/N_1$ (calculated at the die exit for the given shear rate and considering fully developed slit flow) plays an important role (see Figure 10d). This suggests that the Leonov model parameters should be determined by using a uniaxial extensional viscosity data measured at very wide extensional strain rates and utilizing other properties such as planar extensional viscosity, N_1 and N_2, if they are available. A comparison between the uniaxial extensional viscosity data for all five polyethylene samples (taken from [18], [37,38,40] and [47]) and corresponding modified Leonov model predictions for uniaxial as well as planar extensional viscosities is provided in Figure 11. As it can be seen, single-mode modified Leonov model has a capability to describe uniaxial extensional viscosity for all samples.

In the second step, material relaxation time, λ, mean extensional strain rate in the air gap, $\left(\frac{du}{dx}\right)_M$, and shear rate at the die exit (corrected for the non-Newtonian behavior) [70,71] $\dot{\gamma}_{COR}$, were determined for processing conditions and summarized for all samples in Table 6 as follows:

$$\lambda = \lambda(T_0)\exp\left[\frac{E_a}{R}\left(\frac{1}{T}-\frac{1}{T_0}\right)\right] \tag{36}$$

$$\left(\frac{du}{dx}\right)_M = \frac{u-u_0}{X} \tag{37}$$

$$\dot{\gamma}_{COR} = \frac{6Q}{8L_0e_0^2}\left(\frac{2n_0+1}{3n_0}\right) \tag{38}$$

Here $\lambda(T_0)$ represents relaxation time at the reference temperature, T_0, (Table 5), E_a is the flow activation energy (Table 4), R is the universal gas constant equal to 8.3144598 J/K/mol, u is the take-up velocity, u_0 is the die exit velocity, X is the air gap, Q is the overall

volumetric flow rate, L_0 is the die half-width, e_0 is the die half-gap and n_0 is the index of non-Newtonian behavior (equal to 0.3464 as the typical value for LDPEs [72]). The exponential term in Eq. 36 represents Arrhenius shift factor [73,74] whereas the second term in Eq. 38 represents Rabinowitsch correction for a rectangle channel [75]. All parameters appearing in Eq. 31 for the normalized maximum attainable normalized neck-in, NI^*, (i.e. De, $\frac{\eta_{E,U,max}}{3\eta_0}$, $\frac{\eta_{E,P}}{\eta_{E,U}}$ and $-N_2/N_1$ for given processing parameters and materials used) were calculated by using modified Leonov model utilizing λ, $\left(\frac{du}{dx}\right)_M$ and $\dot{\gamma}_{COR}$ parameters determined via Eqs. 36-38 (see their summarization in Table 7).

In the final step, measured values for NI^*, provided in Table 6, were compared with corresponding predictions of approximate model (Eq. 31) utilizing constants and parameters provided in Table 3 and Table 7, respectively (see Figure 12a). As it can be seen, there is a very good agreement between the measured data and approximate model predictions within the whole range of Deborah numbers. If the $-N_2/N_1$ at the die exit region is considered to be unrealistically constant for all tested LDPEs (for example equal to 0.2 as the 'typical value' [76]), the model failed to predict NI^* for Deborah numbers larger than 0.1 (see Figure 12b), which confirms existence of the critical Deborah number, above which, the neck-in phenomenon starts to be strongly dependent on the die exit stress state.

Based on the performed analysis, it can be concluded that the approximate model, which relates the normalized maximum attainable normalized neck-in with De, $\frac{\eta_{E,U,max}}{3\eta_0}$, $\frac{\eta_{E,P}}{\eta_{E,U}}$ and $-N_2/N_1$ according to Eq. 31, can be considered as a useful tool for material, processing and die design optimization in order to suppress unwanted neck-in phenomenon occurring during a production of thin flat films.

5 CONCLUSIONS

In this work, the effect of second to first normal stress difference ratio at the die exit, $-N_2/N_1$, uniaxial extensional strain hardening, $\frac{\eta_{E,U,max}}{3\eta_0}$, planar-to-uniaxial extensional viscosity ratio, $\frac{\eta_{E,P}}{\eta_{E,U}}$, and Deborah number, *De*, has been investigated via viscoelastic isothermal modeling utilizing 1D membrane model and a single-mode modified Leonov model as the constitutive equation. Based on the performed parametric study, it was found that an increase in $-N_2/N_1$ ratio and *De* increases both, the neck-in as well as its sensitivity to $\sqrt{\frac{\eta_{E,P}}{\eta_{E,U}}}$. There exists a threshold value for Deborah number and $\frac{\eta_{E,U,max}}{3\eta_0}$, above which, the neck-in starts to be strongly dependent on the die exit stress state, $-N_2/N_1$. It was found that such critical *De* decreases if $-N_2/N_1$, $\frac{\eta_{E,U,max}}{3\eta_0}$ increases and/or $\frac{\eta_{E,P,max}}{4\eta_0}/\frac{\eta_{E,U,max}}{3\eta_0}$ decreases. Numerical solutions of the 1D membrane viscoelastic model, utilizing modified single-mode Leonov model as the constitutive equation, were successfully approximated by a dimensionless analytical equation expressing the normalized maximum attainable neck-in with $\frac{\eta_{E,U,max}}{3\eta_0}$, $\frac{\eta_{E,P}}{\eta_{E,U}}$, $-N_2/N_1$ and *De*. Suggested equation was tested by using the experimental data taken from [18], [37,38,40] and [47] for five different polyethylenes where $0.011 \le De \le 0.253$, $0.825 \le \frac{\eta_{E,P}}{\eta_{E,U}} \le 1.910$, $2.047 \le \frac{\eta_{E,U,max}}{3\eta_0} \le 10.096$ and $0.017 \le -\frac{N_2}{N_1} \le 0.680$. It was found that approximate model predictions are in a very good agreement with the corresponding experimental data within the whole range of investigated Deborah numbers. Interestingly, the neck-in predictions for Deborah numbers larger than

0.1 became unrealistic, if the $-N_2/N_1$ at the die exit region is not taken into account, which confirms the existence of critical Deborah number, above which, the neck-in phenomenon starts to be strongly dependent on the die exit stress state. It is believed that the obtained knowledge together with the suggested simple analytical model can be used for optimization of the extrusion die design (influencing flow history and thus die exit stress state), molecular architecture of polymer melts and processing conditions to suppress neck-in phenomenon in a production of very thin flat films.

Acknowledgments

The authors wish to acknowledge the financial support from the Grant Agency of the Czech Republic (Grant registration No. 16-05886S).

6 LIST OF SYMBOLS

A	Aspect ratio	1
A_1, A_2	Fitting parameters of analytical model	1
b	Dissipation term	s^{-1}
$\bar{b}$	Dimensionless dissipation term	1
$\underline{\underline{c}}$	Recoverable Finger tensor	1
$\underline{\underline{c}}^{-1}$	Inverse recoverable Finger tensor	1
$\overset{0}{\underline{\underline{c}}}$	Jaumann (corotational) time derivative of the recoverable Finger strain tensor	s^{-1}
c_{xx}	Normal component of the recoverable Finger tensor in axial x-direction	1
c_{yy}	Normal component of the recoverable Finger tensor in transverse y-direction	1
c_{zz}	Normal component of the recoverable Finger tensor in thickness z-direction	1
$\underline{\underline{D}}$	Deformation rate tensor	s^{-1}
De	Deborah number	1
DR	Draw ratio	1
$\underline{\underline{e}}_p$	Irreversible rate of strain tensor	s^{-1}
E	Dimensionless take-up force	1
E_a	Flow activation energy	$J \cdot mol^{-1}$
e	Half-thickness of the film at any x location	mm
e_0	Die half-gap (half-thickness of the film at the die exit)	mm
$\bar{e}$	Dimensionless half-thickness of the film at any *x* location	1
F	Take-up force (stretching force)	N
f	Rate of deformation in transverse y-direction	s^{-1}
G	Linear Hookean elastic modulus	Pa
g	Rate of deformation in thickness z-direction	s^{-1}

i	Index *i*, noting the spatial direction	1
$I_{1,c}$	First invariant of recoverable Finger tensor	1
$I_{2,c}$	Second invariant of recoverable Finger tensor	1
j	Index *j*	1
L	Half-width of the film at any *x* location	mm
L_0	Half-width of the die (half-width of the film at the die exit)	mm
$\bar{L}$	Dimensionless half-width of the film at any x location	1
MFI	Mass flow index	$g \cdot 10\ min^{-1}$
MFR	Mass flow rate	$kg \cdot h^{-1}$
M_n	Number average molar mass	$g \cdot mol^{-1}$
M_w	Mass average molar mass	$g \cdot mol^{-1}$
NI	Maximum attainable neck-in	mm
NI^*	Normalized maximum attainable neck-in	1
N_1	First normal stress difference	Pa
N_2	Second normal stress difference	Pa
n	Non-linear Leonov model parameter	1
n_0	Non-Newtonian index	1
n_s	Number of sample points	1
Q	Volumetric flow rate	$m^3 \cdot s^{-1}$
R	Gas constant	$J \cdot K^{-1} \cdot mol^{-1}$
T	Melt temperature at the die	°C
T_0	Reference temperature in the Arrhenius law	°C
u	Axial velocity component of the film at any *x* location	$mm \cdot s^{-1}$
$u(X)$	Chill roll speed	$mm \cdot s^{-1}$
u_0	Axial velocity component at the die exit	$mm \cdot s^{-1}$
$\bar{u}$	Dimensionless axial velocity component of the film at any *x* location	1

v	Transverse velocity component of the film at any *x* location	$mm \cdot s^{-1}$
W	Elastic potential	Pa
w	Thickness velocity component of the film at any *x* location	$mm \cdot s^{-1}$
X	Take-up length (stretching distance, air gap)	mm
x	Position in axial x-direction	mm
$\bar{x}$	Dimensionless position in axial x-direction	1
y_i	Observed value	1
$\hat{y}_i$	Predicted value	1
x, y, z	Spatial coordinates in axial, transverse and thickness direction, respectively	1
Z_x, Z_y, Z_z	Substitution variables	1
$\left(\frac{du}{dx}\right)_M$	Mean value of extensional strain rate in the air gap	s^{-1}
$\frac{dc_{xx}}{d\bar{x}}, \frac{dc_{yy}}{d\bar{x}}, \frac{dc_{zz}}{d\bar{x}}$	Derivative of Finger tensor components with respect to dimensionless $\bar{x}$ position	1
$\frac{d\bar{u}}{d\bar{x}}, \frac{d\bar{L}}{d\bar{x}}, \frac{d\bar{e}}{d\bar{x}}$	Derivative of dimensionless axial, transverse and thickness velocity component with respect to dimensionless $\bar{x}$ position	1

Greek Symbols

α	Arrhenius law parameter	K
α_1, α_2	Fitting parameters of analytical model	1
β	Non-linear Leonov model parameter	1
$\dot{\gamma}_{COR}$	Corrected shear rate by Rabinowitsch correction for the rectangle channel	s^{-1}
$\underline{\underline{\delta}}$	Unit tensor (Kronecker delta)	1
δ	δ shift function	1
η_0	Newtonian viscosity	Pa·s
$\eta_{E,P}$	Steady planar extensional viscosity	Pa·s

$\eta_{E,P,max}$	Maximal steady planar extensional viscosity	Pa·s
$\eta_{E,U}$	Steady uniaxial extensional viscosity	Pa·s
$\eta_{E,U,max}$	Maximal steady uniaxial extensional viscosity	Pa·s
θ	Fitting parameters of analytical model	1
λ	Relaxation time	s
ν	Non-linear Leonov model parameter	1
ξ	Non-linear Leonov model parameter	1
ρ	Polymer density	$g \cdot cm^{-3}$
$\underline{\underline{\tau}}$	Extra stress tensor	Pa
τ_{xx}	Normal stress in axial x-direction	Pa
τ_{yy}	Normal stress in transverse y-direction	Pa
τ_{zz}	Normal stress in thickness z-direction	Pa
$\bar{\tau}_{xx}$	Dimensionless normal stress in axial x-direction	1
$\bar{\tau}_{yy}$	Dimensionless normal stress in transverse y-direction	1
$\bar{\tau}_{zz}$	Dimensionless normal stress in thickness z-direction	1
φ_1, φ_2	Fitting parameters of analytical model	1
$\psi_1, \psi_2, \psi_3, \psi_4$	Fitting parameters of analytical model	1

7 REFERENCES

[1] T. Kanai, G.A. Campbell, Film Processing Advances, Second Edi, Hanser Publishers, Munich, 2014.

[2] T. Kanai, G.A. Campbell, Film Processing, Hanser Publishers, Munich, 1999.

[3] R.J. Fisher, M.M. Denn, Finite-amplitude stability and draw resonance in isothermal melt spinning, Chem. Eng. Sci. 30 (1975) 1129–1134.

[4] R.J. Fisher, M.M. Denn, A theory of isothermal melt spinning and draw resonance, AIChE J. 22 (1976) 236–246.

[5] D. Gelder, The stability of fiber drawing processes, Ind. Eng. Chem. Fundam. 10 (1971) 534–535.

[6] Y.L. Yeow, On the stability of extending films: a model for the film casting process, J. Fluid Mech. 66 (1974) 613–622.

[7] G.R. Aird, Y.L. Yeow, Stability of film casting of power-law liquids, Ind. Eng. Chem. Fundam. 22 (1983) 7–10.

[8] N.R. Anturkar, A. Co, Draw resonance in film casting of viscoelastic fluids: A linear stability analysis, J. Nonnewton. Fluid Mech. 28 (1988) 287–307.

[9] V.R. Iyengar, A. Co, Film casting of a modified Giesekus fluid: a steady-state analysis, J. Nonnewton. Fluid Mech. 48 (1993) 1–20.

[10] V.R. Iyengar, A. Co, Film casting of a modified Giesekus fluid: Stability analysis, Chem. Eng. Sci. 51 (1996) 1417–1430.

[11] J.P. Sergent, Etude de deux procédés de fabrication de films. Le soufflage de gaine. L'extrusion de film à plat., in: Strasbourg, France, 1977.

[12] D. Cotto, P. Duffo, J.M. Haudin, Cast film extrusion of polypropylene films, Int. Polym. Process. 4 (1989) 103–113.

[13] P. Duffo, B. Monasse, J.M. Haudin, Cast film extrusion of polypropylene. Thermomechanical and physical aspects, J. Polym. Eng. 10 (1991) 151–229.

[14] P. Barq, J.M. Haudin, J.F. Agassant, Isothermal and anisothermal models for cast film extrusion, Int. Polym. Process. 7 (1992) 334–349.

[15] S. D'Halewyu, J.F. Agassant, Y. Demay, Numerical simulation of the cast film process, Polym. Eng. Sci. 30 (1990) 335–340.

[16] B. Debbaut, J.M. Marchal, M.J. Crochet, Viscoelastic effects in film casting, Zeitschrift Für Angew. Math. Und Phys. 46 (1995) 679–698.

[17] W.S. Smith, Simulating the cast film process using an updated Lagrangian finite element algorithm, McMaster University, 2001.

[18] N. Satoh, H. Tomiyama, T. Kajiwara, Viscoelastic simulation of film casting process for a polymer melt, Polym. Eng. Sci. 41 (2001) 1564–1579.

[19] O.S. Narayanaswamy, A One-Dimensional Model of Stretching Float Glass, J. Am. Ceram. Soc. 60 (1977) 1–5.

[20] D. Silagy, Y. Demay, J.F. Agassant, Study of the stability of the film casting process, Polym. Eng. Sci. 36 (1996) 2614–2625.

[21] D. Silagy, Y. Demay, J.F. Agassant, Stationary and stability analysis of the film casting process, J. Nonnewton. Fluid Mech. 79 (1998) 563–583.

[22] K. Sakaki, R. Katsumoto, T. Kajiwara, K. Funatsu, Three-dimensional flow simulation of a film-casting process, Polym. Eng. Sci. 36 (1996) 1821–1831.

[23] H. Zheng, W. Yu, C. Zhou, H. Zhang, Three-Dimensional Simulation of the Non-Isothermal Cast Film Process of Polymer Melts, J. Polym. Res. 13 (2006) 433–440.

[24] G. Lamberti, G. Titomanlio, V. Brucato, Measurement and modelling of the film casting process 1. Width distribution along draw direction, Chem. Eng. Sci. 56 (2001) 5749–5761.

[25] G. Lamberti, G. Titomanlio, V. Brucato, Measurement and modelling of the film casting process 2. Temperature distribution along draw direction, Chem. Eng. Sci. 57 (2002) 1993–1996.

[26] G. Lamberti, V. Brucato, G. Titomanlio, Orientation and crystallinity in film casting of polypropylene, J. Appl. Polym. Sci. 84 (2002) 1981–1992.

[27] G. Lamberti, F. De Santis, V. Brucato, G. Titomanlio, Modeling the interactions between light and crystallizing polymer during fast cooling, Appl. Phys. A. 78 (2004) 895–901.

[28] G. Lamberti, Flow-induced crystallization during isotactic polypropylene film casting, Polym. Eng. Sci. 51 (2011) 851–861.

[29] G. Titomanlio, G. Lamberti, Modeling flow induced crystallization in film casting of polypropylene, Rheol. Acta. 43 (2004) 146–158.

[30] G. Lamberti, G. Titomanlio, Analysis of film casting process: The heat transfer phenomena, Chem. Eng. Process. Process Intensif. 44 (2005) 1117–1122.

[31] G. Lamberti, G. Titomanlio, Analysis of Film Casting Process : Effect of Cooling during the Path in Air, Ind. Eng. Chem. Res. 45 (2006) 719–723.

[32] H. Ito, M. Doi, T. Isaki, M. Takeo, K. Yagi, 2D Flow Analysis of Film Casting Process, J. Soc. Rheol. Japan. 31 (2003) 149–155.

[33] H. Ito, M. Doi, T. Isaki, M. Takeo, A Model of Neck-in Phenomenon in Film Casting Process, J. Soc. Rheol. Japan. 31 (2003) 157–163.

[34] C.W. Seay, D.G. Baird, Sparse Long-chain Branching's Effect on the Film-casting Behavior of PE, Int. Polym. Process. 24 (2009) 41–49.

[35] C.D. McGrady, C.W. Seay, D.G. Baird, Effect of sparse long-chain branching on the film-casting behavior for a series of well-defined HDPEs, Int. Polym. Process. 24 (2009) 428–438.

[36] H. Kometani, T. Matsumura, T. Suga, T. Kanai, Experimental and theoretical analyses of film casting process, J. Polym. Eng. 27 (2007) 1–28.

[37] H.V. Pol, S.S. Thete, P. Doshi, A.K. Lele, Necking in extrusion film casting: The role of macromolecular architecture, J. Rheol. (N. Y. N. Y). 57 (2013) 559–583.

[38] H.V. Pol, S. Banik, L.B. Azad, S.S. Thete, P. Doshi, A. Lele, Nonisothermal analysis of extrusion film casting process using molecular constitutive equations, Rheol. Acta. 53 (2014) 85–101.

[39] K. Chikhalikar, S. Banik, L.B. Azad, K. Jadhav, S. Mahajan, Z. Ahmad, S. Kulkarni, S. Gupta, P. Doshi, H.V. Pol, A. Lele, Extrusion film casting of long chain branched polypropylene, Polym. Eng. Sci. 55 (2015) 1977–1987.

[40] S.S. Thete, P. Doshi, H.V. Pol, New insights into the use of multi-mode phenomenological constitutive equations to model extrusion film casting process, J. Plast. Film Sheeting. 33 (2017) 35–71.

[41] R. Dhadwal, S. Banik, P. Doshi, H.V. Pol, Effect of viscoelastic relaxation modes on stability of extrusion film casting process modeled using multi-mode Phan-Thien-Tanner constitutive equation, Appl. Math. Model. 47 (2017) 487–500.

[42] H.V. Pol, S.S. Thete, Necking in Extrusion Film Casting: Numerical Predictions of the Maxwell Model and Comparison with Experiments, J. Macromol. Sci. Part B. 55 (2016) 984–1006.

[43] T. Dobroth, L. Erwin, Causes of edge beads in cast films, Polym. Eng. Sci. 26 (1986) 462–467.

[44] N. Toft, M. Rigdahl, Extrusion coating with metallocene-catalysed polyethylenes, Int. Polym. Process. 17 (2002) 244–253.

[45] S. Kouda, Prediction of processability at extrusion coating for low-density polyethylene, Polym. Eng. Sci. 48 (2008) 1094–1102.

[46] S. Shiromoto, Y. Masutani, M. Tsutsubuchi, Y. Togawa, T. Kajiwara, A neck-in model in extrusion lamination process, Polym. Eng. Sci. 50 (2010) 22–31.

[47] S. Shiromoto, Y. Masutani, M. Tsutsubuchi, Y. Togawa, T. Kajiwara, The effect of viscoelasticity on the extrusion drawing in film-casting process, Rheol. Acta. 49 (2010) 757–767.

[48] S. Shiromoto, The Mechanism of Neck-in Phenomenon in Film Casting Process, Int. Polym. Process. 29 (2014) 197–206.

[49] K. Christodoulou, S.G. Hatzikiriakos, D. Vlassopoulos, Stability analysis of film casting for PET resins using a multimode Phan-Thien-Tanner constitutive equation, J. Plast. Film Sheeting. 16 (2000) 312–332.

[50] S. Smith, D. Stolle, Numerical Simulation of Film Casting Using an Updated Lagrangian Finite Element Algorithm, Polym. Eng. Sci. 43 (2003) 1105–1122.

[51] S. Bourrigaud, G. Marin, V. Dabas, C. Dupuy, D. Silagy, The draw ratio–Deborah number diagram: A useful tool for coating applications, Polym. Eng. Sci. 46 (2006) 372–380.

[52] J.M. Kim, J.S. Lee, D.M. Shin, H.W. Jung, J.C. Hyun, Transient solutions of the dynamics of film casting process using a 2-D viscoelastic model, J. Nonnewton. Fluid Mech. 132 (2005) 53–60.

[53] T. Kajiwara, M. Yamamura, T. Asahina, Relationship between Neck-in Phenomena and Rheological Properties in Film Casting, Nihon Reoroji Gakkaishi. 34 (2006) 97–103.

[54] M.E. Pis-Lopez, A. Co, Multilayer film casting of modified Giesekus fluids Part 1. Steady-state analysis, J. Nonnewton. Fluid Mech. 66 (1996) 71–93.

[55] T. Barborik, M. Zatloukal, C. Tzoganakis, On the Role of Extensional Rheology and Deborah Number on the Neck-in Phenomenon During Flat Film Casting, Int. J. Heat Mass Transf. 111 (2017) 1296–1313.

[56] V.R. Iyengar, Film casting of polymer melts, University of Maine, 1993.

[57] G. Oliver, Internally deckled coating dies, in: TAPPI Eur. PLACE Conf., Athens; Greece, 2007: pp. 311–339.

[58] M. Zatloukal, R. Kolarik, Investigation of convective heat transfer in 9-layer film blowing process by using variational principles, Int. J. Heat Mass Transf. 86 (2015) 258–267.

[59] J. Musil, M. Zatloukal, Effect of die exit geometry on internal die drool phenomenon during linear HDPE melt extrusion, Int. J. Heat Mass Transf. 56 (2013) 667–673.

[60] R. Kolarik, M. Zatloukal, M. Martyn, The effect of polyolefin extensional rheology on non-isothermal film blowing process stability, Int. J. Heat Mass Transf. 56 (2013) 694–708.

[61] A.I. Leonov, Nonequilibrium Thermodynamics and Rheology of Viscoelastic Polymer Media, Rheol. Acta. 15 (1976) 85–98.

[62] A.I. Leonov, E.H. Lipkina, E.D. Paskhin, A.N. Prokunin, Theoretical and experimental investigation of shearing in elastic polymer liquids, Rheol. Acta. 15 (1976) 411–426.

[63] A.I. Leonov, A.N. Prokunin, An improved simple version of a nonlinear theory of elasto-viscous polymer media, Rheol. Acta. 19 (1980) 393–403.

[64] A.I. Leonov, A.N. Prokunin, On nonlinear effects in the extensional flow of polymeric liquids, Rheol. Acta. 22 (1983) 137–150.

[65] M. Simhambhatla, A.I. Leonov, On the rheological modeling of viscoelastic polymer liquids with stable constitutive equations, Rheol. Acta. 34 (1995) 259–273.

[66] A.I. Leonov, Constitutive equations for viscoelastic liquids: Formulation, analysis and comparison with data, Rheol. Ser. 8 (1999) 519–575.

[67] M. Zatloukal, Differential viscoelastic constitutive equations for polymer melts in steady shear and elongational flows, J. Nonnewton. Fluid Mech. 113 (2003) 209–227.

[68] M. Beaulne, E. Mitsoulis, Numerical Simulation of the Film Casting Process, Int. Polym. Process. 14 (1999) 261–275.

[69] J. Drabek, M. Zatloukal, Evaluation of Thermally Induced Degradation of Branched Polypropylene by Using Rheology and Different Constitutive Equations, Polymers (Basel). 8 (2016) 317.

[70] C.W. Macosko, Rheology : principles, measurements, and applications, VCH, 1994.

[71] J. Vlachopoulos, J.R. Wagner, The SPE Guide on Extrusion Technology and Troubleshooting, The Society of Plastics Engineers, Brookfield, 2001.

[72] M. Zatloukal, Measurements and modeling of temperature-strain rate dependent uniaxial and planar extensional viscosities for branched LDPE polymer melt, Polymer (Guildf). 104 (2016) 258–267.

[73] J.D. Ferry, Viscoelastic properties of polymers, 3rd edit., John Wiley & Sons, New York, 1980.

[74] J.M. Dealy, R.G. Larson, Structure and Rheology of Molten Polymers - From Structure to Flow Behavior and Back Again, Hanser Publishers, Munich, 2006.

[75] C.W. Macosko, Rheology: principles, measurements, and applications, Wiley, New York, NY, 1994.

[76] E.A. Jensen, J. deC. Christiansen, Measurements of first and second normal stress differences in a polymer melt, J. Nonnewton. Fluid Mech. 148 (2008) 41–46.

8 TABLES

Table 1. Summarization of utilized dimensionless quantities.

Dimensionless component of stress tensor
$\bar{\tau}_{ii} = \frac{\tau_{ii} e_0 L_0}{F}$
Dimensionless spatial dimensions and streamwise velocity
$\bar{x} = \frac{x}{X} \qquad \bar{e} = \frac{e}{e_0} \qquad \bar{L} = \frac{L}{L_0} \qquad \bar{u} = \frac{u}{u_0}$
Dimensionless numbers
$DR = \frac{u(X)}{u_0} \qquad De = \frac{\lambda u_0}{X} \qquad A = \frac{X}{L_0} \qquad \frac{1}{E} = \frac{FX}{G\lambda e_0 L_0 u_0}$

Table 2. Modified Leonov model parameters for the utilized virtual polymer melts having $\lambda = 1.57\ s$ and $G = 85{,}982.61\ Pa$ at 150 °C.

Virtual Material Name	$\boldsymbol{\xi}$ (1)	$\boldsymbol{\nu}$ (1)	$\boldsymbol{\beta}$ (1)	$\frac{\eta_{E,U,max}}{3\eta_0}$ (1)	$\frac{\eta_{E,P,max}}{4\eta_0}$ (1)	$\lim_{\dot{\gamma}\to 0}\left(-\frac{N_2}{N_1}\right)$ (1)
Melt1_High	4.414	0.276	0.1	7.1	6.2	0.3
Melt2_High	4.042	0.208	0.3	7.1	6.6	0.4
Melt3_High	3.816	0.174	0.4	7.1	6.8	0.45
Melt4_High	3.54	0.14	0.5	7.1	7.1	0.5
Melt5_High	2.806	0.072	0.7	7.1	7.9	0.6
Melt1_Middle	2.014	0.276	0.1	3.4	2.9	0.3
Melt2_Middle	1.882	0.208	0.3	3.4	3.1	0.4
Melt3_Middle	1.816	0.174	0.4	3.4	3.2	0.45
Melt4_Middle	1.75	0.14	0.5	3.4	3.4	0.5
Melt5_Middle	1.53	0.072	0.7	3.4	4.2	0.6
Melt1_Low	0.338	0.276	0.1	1.3	1.10	0.3
Melt2_Low	0.38	0.208	0.3	1.3	1.17	0.4
Melt3_Low	0.4	0.174	0.4	1.3	1.22	0.45
Melt4_Low	0.418	0.14	0.5	1.3	1.29	0.5
Melt5_Low	0.426	0.072	0.7	1.3	1.53	0.6

Table 3. Summarization of all constants appearing in Eq. 31 for normalized maximum attainable neck-in, NI^*, which was used to fit all numerical neck-in predictions. The root mean square error, *RMSE*, was equal to 0.020888 .

θ	A_1	A_2	α_1	α_2	φ_1	φ_2	Ψ_1	Ψ_2	Ψ_3	Ψ_4
7.43	0.593	1.027	1073.742	0.849	2.113	0.514	1.027	0.849	0.514	3.953

Table 4. Basic characteristics for tested polymeric samples.

Polymer sample	**MFI** (g/10 min)	M_w (kg/mol)	M_w/M_n (1)	**Newtonian viscosity,** η_0 (Pa·s)	**Temperature,** T_0 (°C)	**Flow activation energy,** E_a (kJ/mol)	**Reference**
LDPE 170A	0.7	185.9	6.07	134,992	150	40	[38,40]
PE-A	6.7	163	9.1	16,220	130	49.887[#]	[47]
PE-B	4.1	102	6.6	37,720	130	49.887[#]	[47]
PE-C	4.3	85	6.0	36,033	130	49.887[#]	[47]
LDPE C	8.07	554	26	21,970	125	52.020[##]	[18]

[#] Note, that E_a was calculated here as $E_a = \alpha R$, where α is the Arrhenius law parameter equal to 6000 K provided in [47] and R is the universal gas constant equal to 8.3144598 J/K/mol.

[##] Converted from Kcal/mol.

Table 5. Modified Leonov model parameters for polymeric materials with basic characteristics provided in Table 4.

Polymer sample	λ (s)	**G** (Pa)	ξ (1)	ν (1)	β (1)	T_0 (°C)
LDPE 170A	1.57	85,982.61	1.53	0.072	0.7	150
PE-A[#]	9.5	1,707.37	0.41	0.0015	0.4	130
PE-B[#]	15	2,514.67	0.29	0.0034	0.4	130
PE-C[#]	30	1,201.10	0.09	0.0013	0.5	130
LDPE C	28.57	768.95	0.51	0.004	0	125

[#] Parameters are taken from [55]**.**

Table 6. Summarization of extrusion film casting processing parameters for all considered polymer samples taken from the open literature [18], [37] and [47].

Polymer sample	**Die Width, $2L_0$** (mm)	**Die Gap, $2e_0$** (mm)	**Air Gap, X** (mm)	**Temperature, T** (°C)	**Die Exit Velocity, u_0** (mm/s)	**Draw Ratio, DR** (1)	**NI*** (1)	**Reference**
LDPE 170A	100	0.46	228	190	4.3	17.1	0.1537	[37]
PE-A	600	0.80	160	320	46.6#	42.9##	0.2466	[47]
PE-B	600	0.80	190	320	46.6#	42.9##	0.3275	[47]
PE-C	600	0.80	220	320	46.6#	42.9##	0.5159	[47]
LDPE C	250	0.95	90	190	5.1	65.2###	0.2973	[18]
LDPE 170A	100	0.46	10	190	4.3	9.6	0.7867	[37]

Die exit velocity was determined based on the die width ($2L_0$), die gap ($2e_0$), melt density (ρ) and mass flow rate (*MFR*) as $u_0 = MFR/(\rho 2L_0 2e_0)$, where $MFR = 60\ kg/h$ and melt density $\rho = 745\ kg/m^3$ [47].

Draw ratio was determined from die exit velocity and take-up velocity as $DR = u/u_0$. Take-up velocity is provided in [47] as $u = 120\ m/min$.

Calculated based on a take-up velocity at the drawing drum.

Table 7. Summarization of all parameters appearing in Eq. 31 for the normalized maximum attainable normalized neck-in (i.e. *De*, $\frac{\eta_{E,U,max}}{3\eta_0}$, $\frac{\eta_{E,P}}{\eta_{E,U}}$ and $-N_2/N_1$) calculated by using modified Leonov model utilizing material relaxation time, λ, mean extensional strain rate in the air gap, $\left(\frac{du}{dx}\right)_M$, and shear rate at the die exit (corrected for the non-Newtonian behavior), $\dot{\gamma}_{COR}$, determined for processing conditions summarized for all samples in Table 6.

Polymer sample	λ (s)	$\left(\frac{du}{dx}\right)_M$ (1/s)	$\dot{\gamma}_{COR}$ (1/s)	**De** (1)	$-N_2/N_1$ (1)	$\frac{\eta_{E,P}}{\eta_{E,U}}$ (1)	$\frac{\eta_{E,U,max}}{3\eta_0}$ (1)
LDPE 170A	0.588	0.300	91.363	0.011	0.680	1.547	3.393
PE-A	0.079	10.281	569.402	0.019	0.405	0.833	9.299
PE-B	0.125	8.879	569.402	0.026	0.406	1.102	4.198
PE-C	0.250	10.281	569.402	0.061	0.500	1.293	2.047
LDPE C	3.149	3.638	52.469	0.178	0.017	0.825	10.096
LDPE 170A	0.588	3.707	91.363	0.253	0.680	1.910	3.393

9 FIGURES

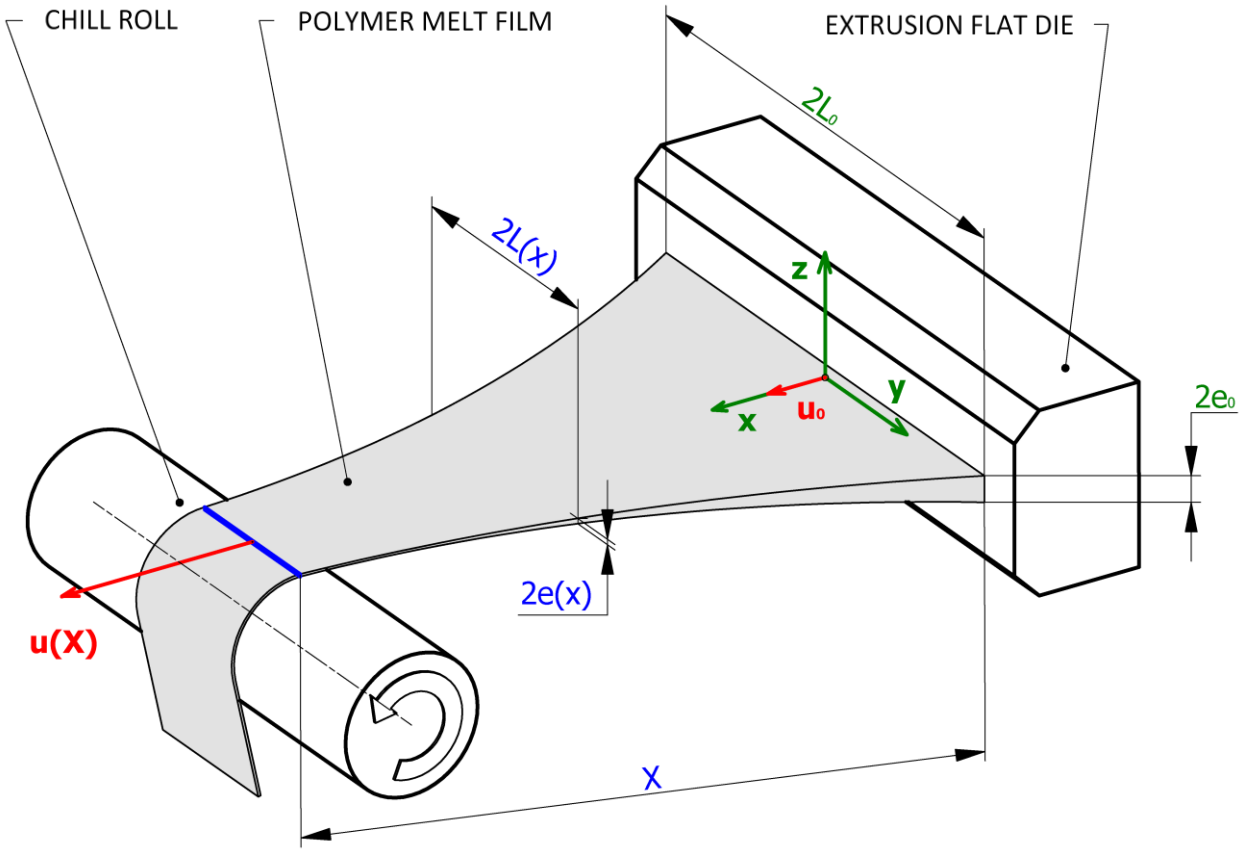

Fig. 1. Schematic visualization of the extrusion film casting process.

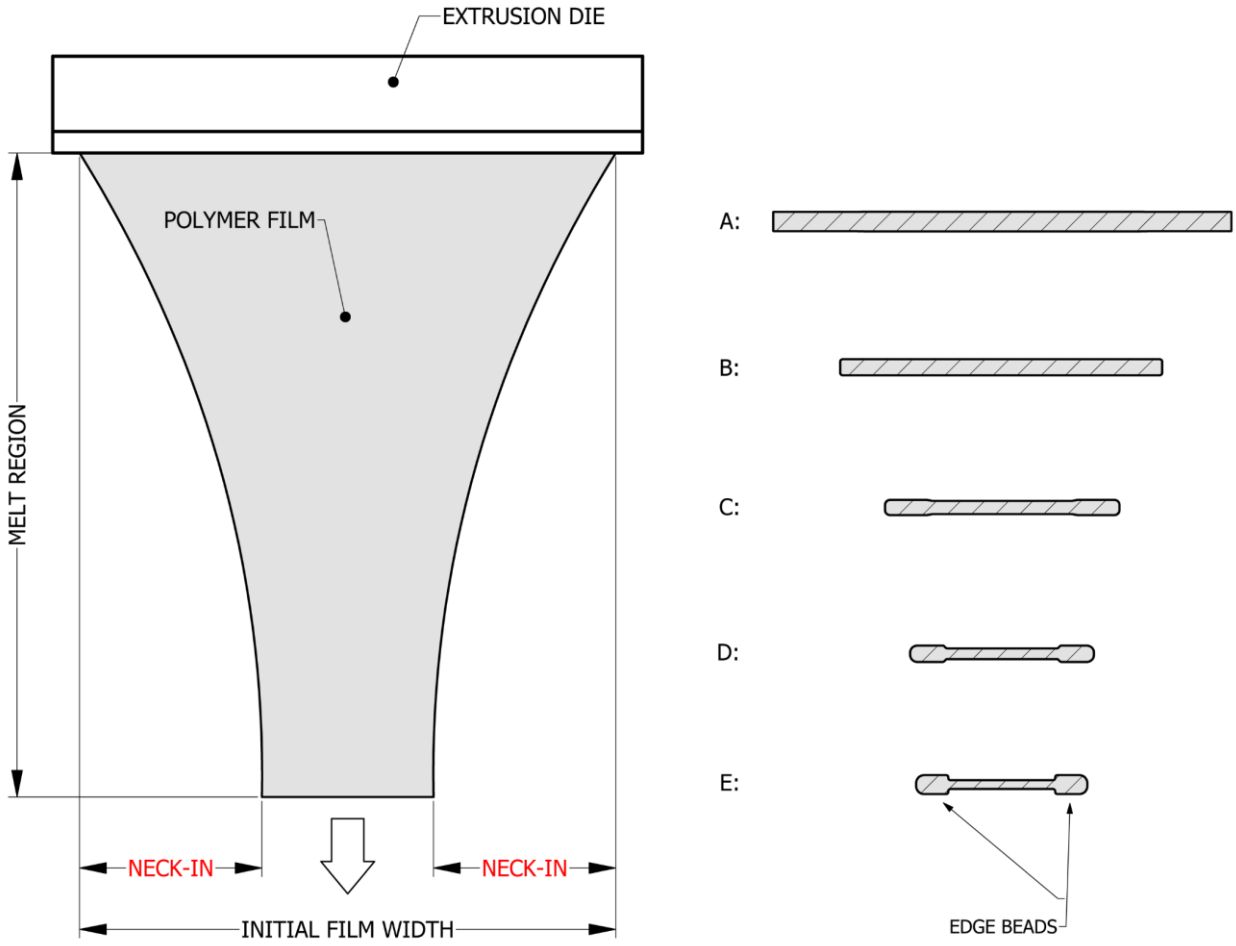

Fig. 2. Neck-in and edge-beading phenomena during the extrusion film casing process.

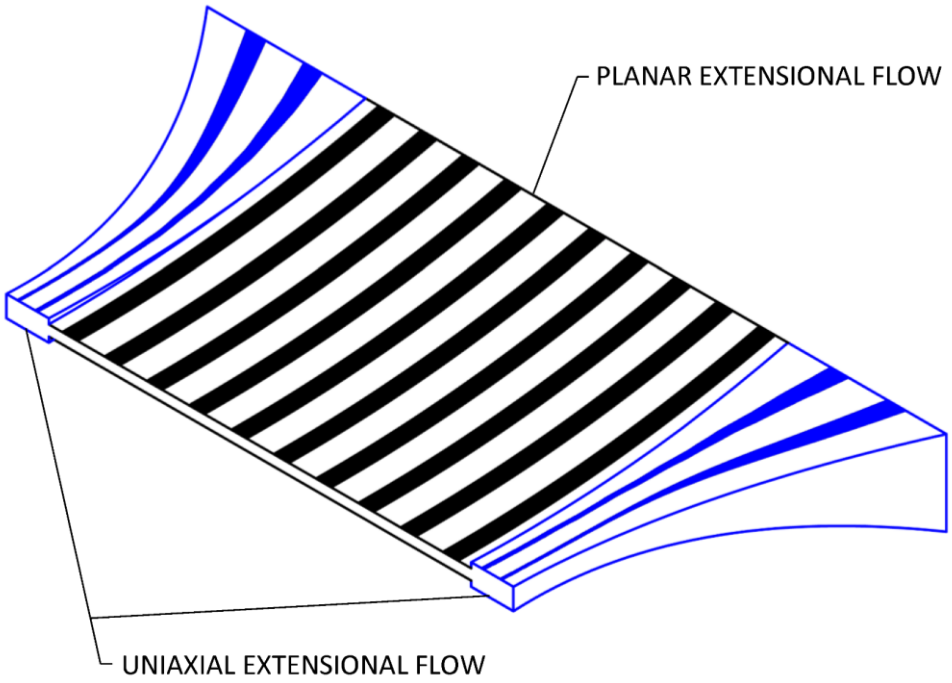

Fig. 3. Visualization of the flow type distribution in the post-die area during the extrusion film casting process.

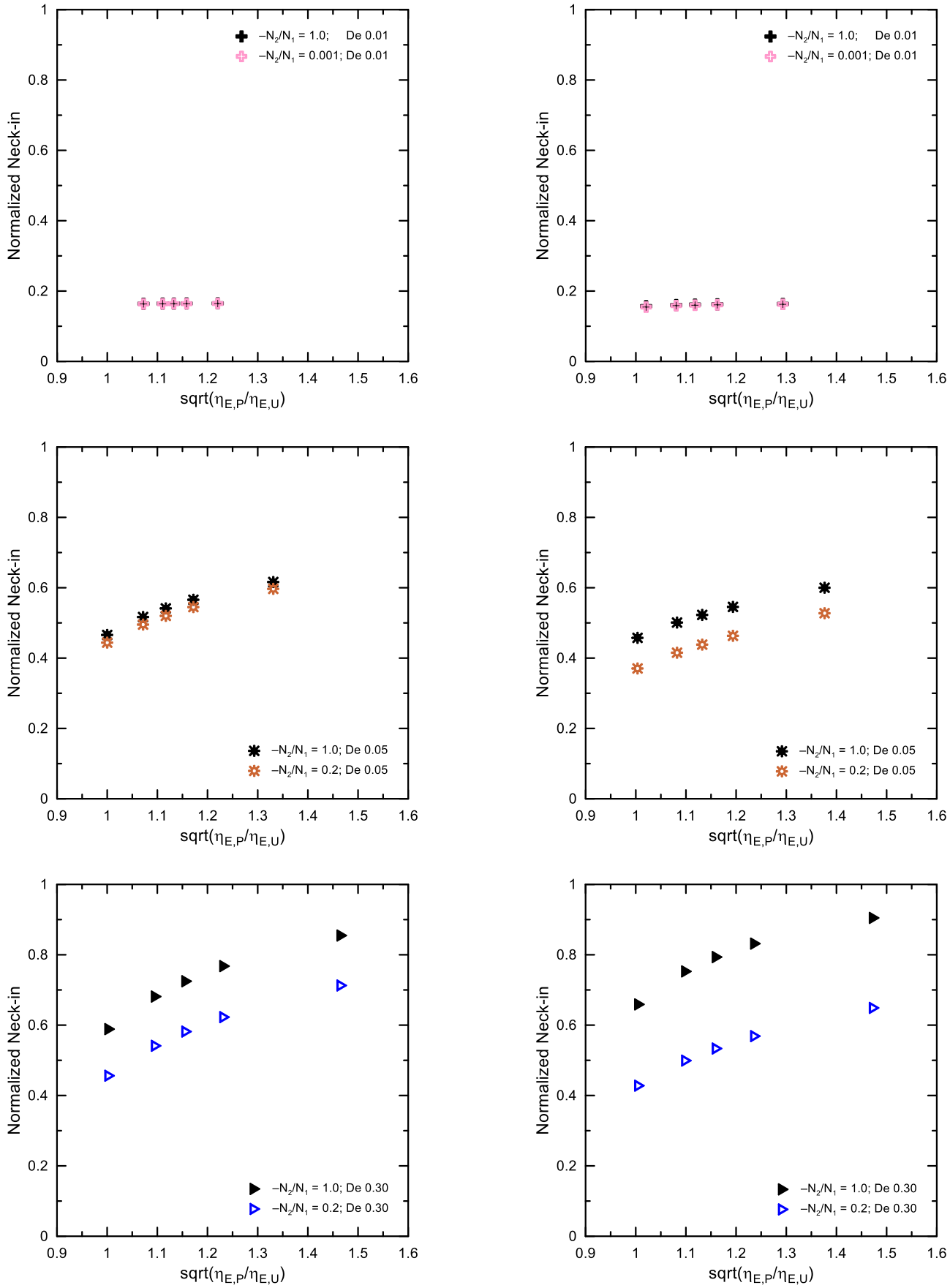

Fig. 4 The effect of die exit stress state ($-N_2/N_1$) on the normalized maximum attainable neck-in vs. $sqrt(\eta_{E,P}/\eta_{E,U})$ dependence for three different Deborah numbers ($De = 0.01$ – top, $De = 0.05$ – middle, $De = 0.3$ – bottom) and two virtual polymer melts having low (left) and high (right) uniaxial extensional strain hardening, $\frac{\eta_{E,U,max}}{3\eta_0}$, equal to 1.3 and 7.1, respectively.

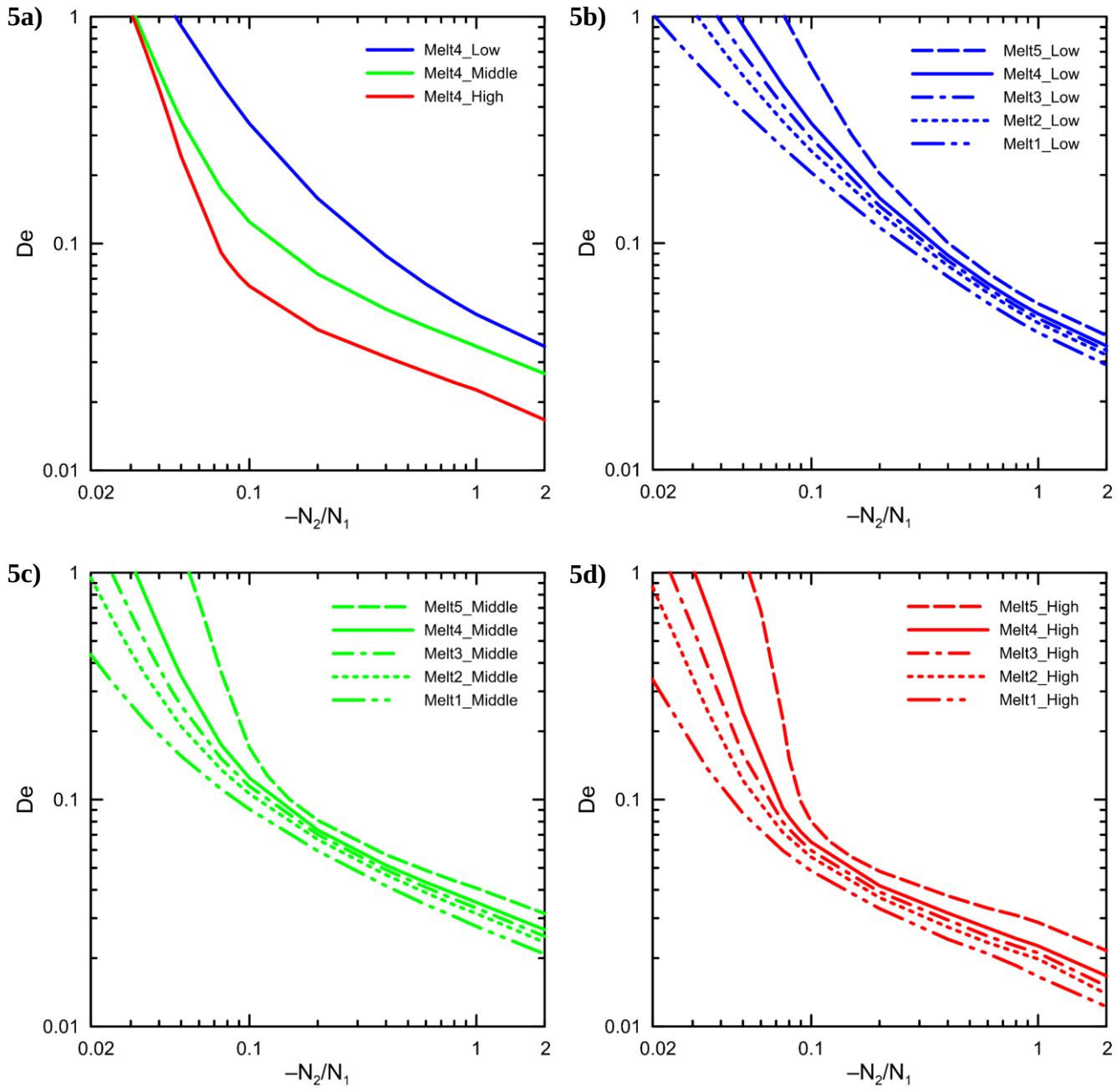

Fig. 5 The effect of die exit stress state ($-N_2/N_1$) on the critical Deborah number, above which, 5% deviation in normalized maximum attainable neck-in starts to occur. **5a)** Role of uniaxial extensional strain hardening, $\frac{\eta_{E,U,max}}{3\eta_0}$, (keeping ratio of planar to uniaxial extensional strain hardening value, $\frac{\eta_{E,P,max}}{4\eta_0}/\frac{\eta_{E,U,max}}{3\eta_0}$, the same, equal to one). **5b)-5d)** Role of $\frac{\eta_{E,P,max}}{4\eta_0}/\frac{\eta_{E,U,max}}{3\eta_0}$ (changing from 0.85 to 1.24) at fixed $\frac{\eta_{E,U,max}}{3\eta_0}$, equal to 1.3 (top, right), 3.4 (bottom, left) and 7.1 (bottom, right).

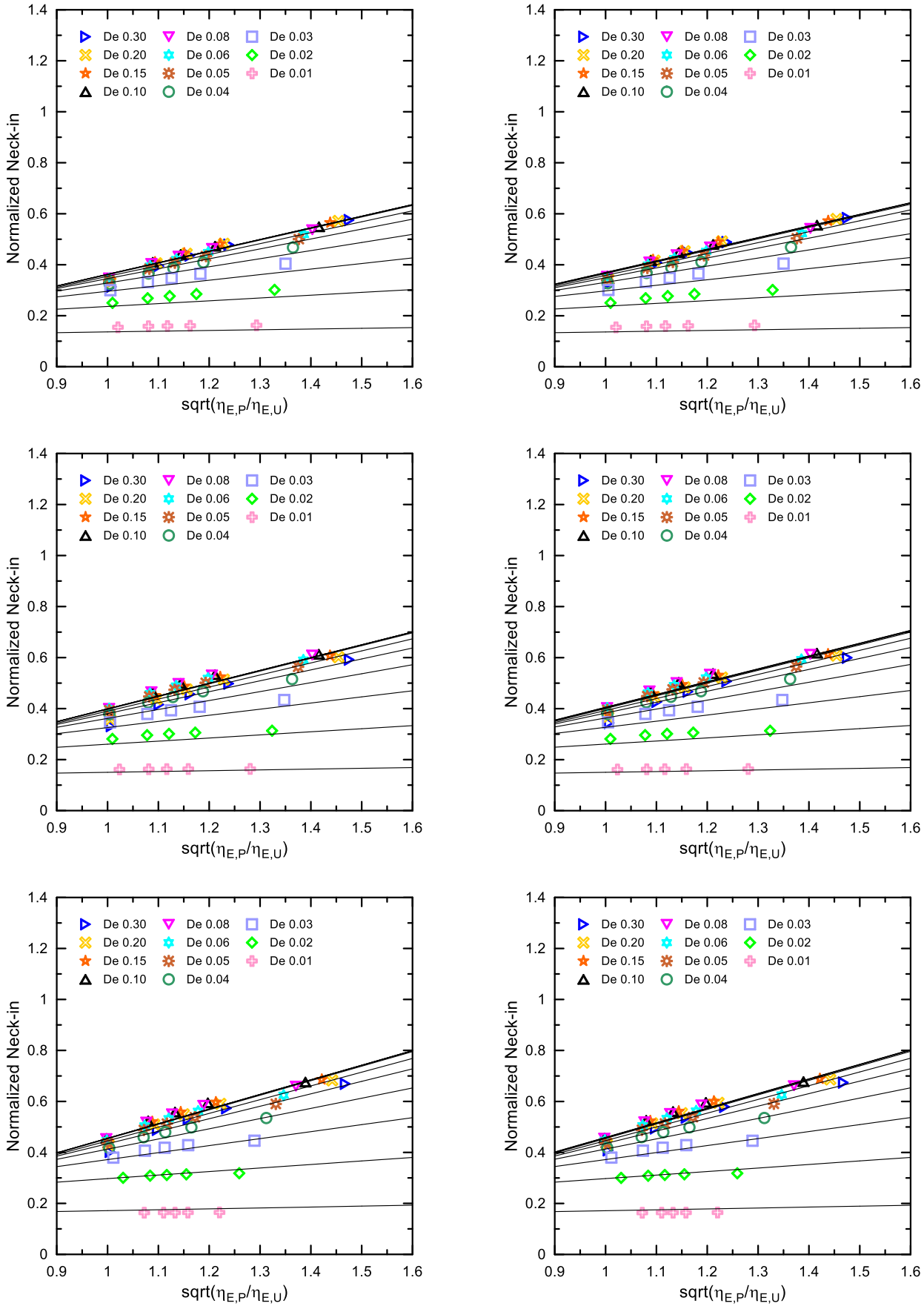

Fig. 6 The effect of Deborah number on the normalized maximum attainable neck-in vs. planar to uniaxial extensional viscosity ratio for virtual polymer melts having high (top), medium (middle) and low (bottom) level of uniaxial extensional strain hardening considering that die exit stress state, $-N_2/N_1$, is equal to 0.001 (left) and 0.02 (right). Here, symbols and lines represent utilized viscoelastic 1D membrane model and simple approximate solution model (Eq. 31) predictions, respectively.

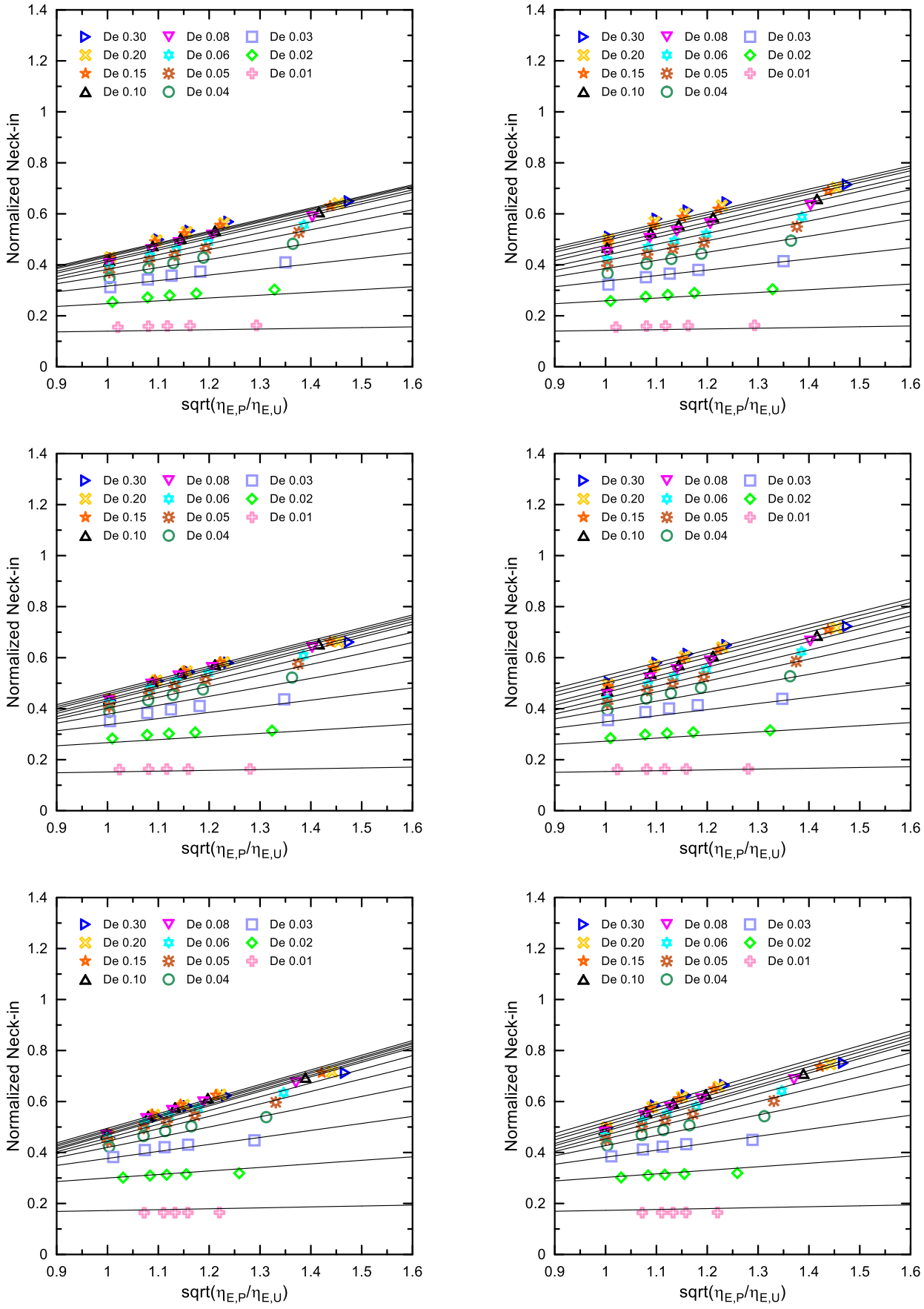

Fig. 7 The effect of Deborah number on the normalized maximum attainable neck-in vs. planar to uniaxial extensional viscosity ratio for virtual polymer melts having high (top), medium (middle) and low (bottom) level of uniaxial extensional strain hardening considering that die exit stress state, $-N_2/N_1$, is equal to 0.2 (left) and 0.4 (right). Here, symbols and lines represent utilized viscoelastic 1D membrane model and simple approximate solution model (Eq. 31) predictions, respectively.

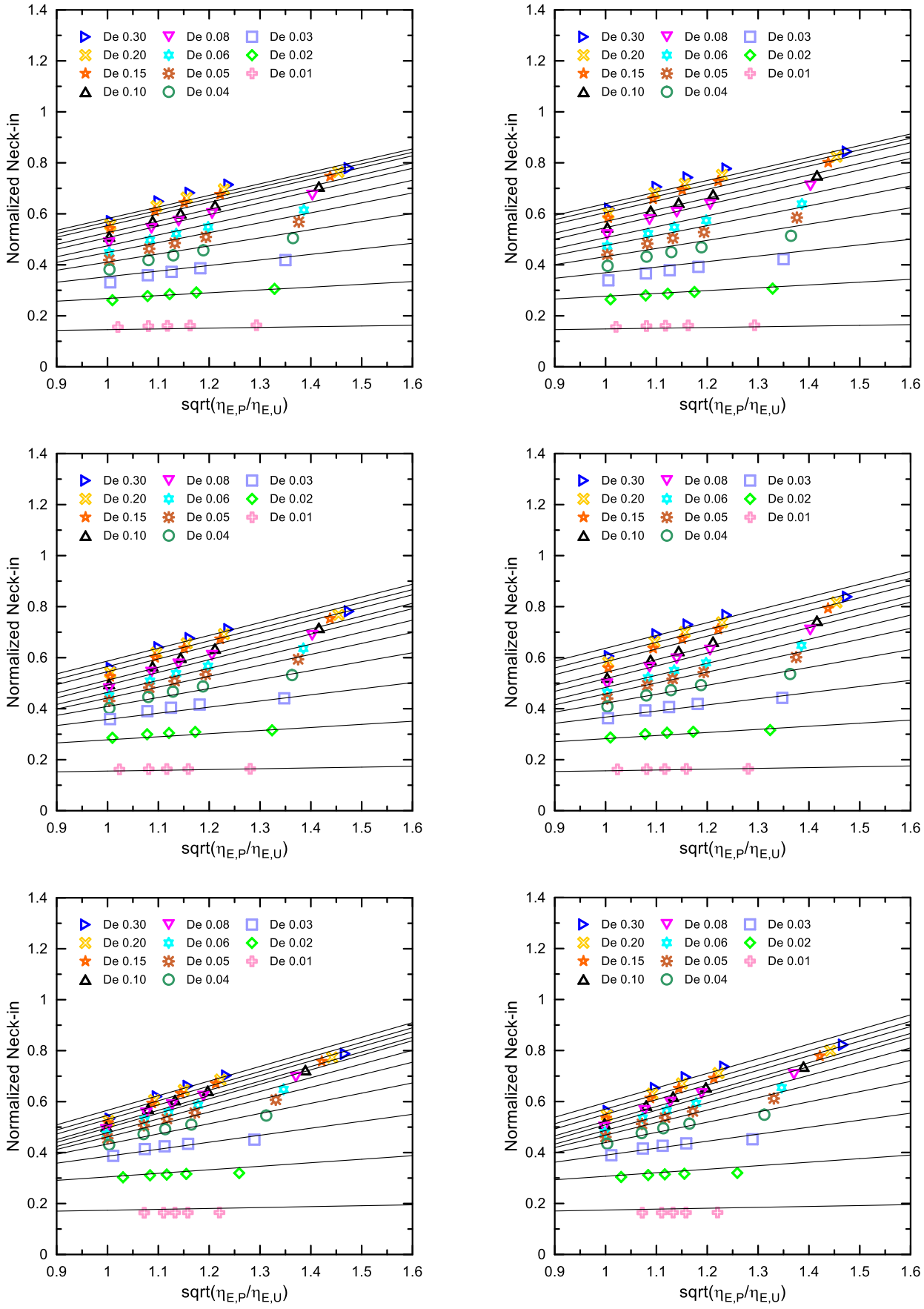

Fig. 8 The effect of Deborah number on the normalized maximum attainable neck-in vs. planar to uniaxial extensional viscosity ratio for virtual polymer melts having high (top), medium (middle) and low (bottom) level of uniaxial extensional strain hardening considering that die exit stress state, $-N_2/N_1$, is equal to 0.6 (left) and 0.8 (right). Here, symbols and lines represent utilized viscoelastic 1D membrane model and simple approximate solution model (Eq. 31) predictions, respectively.

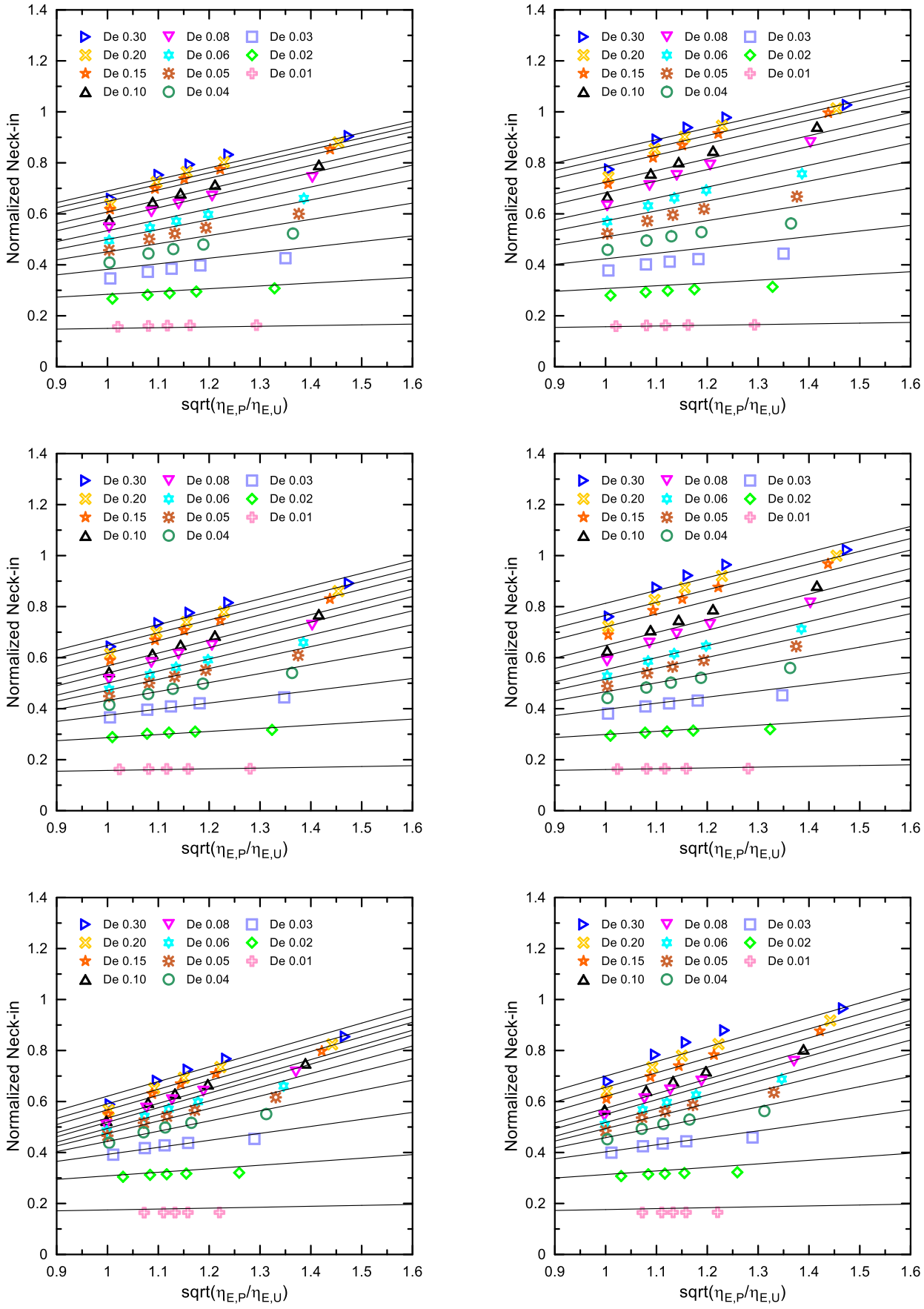

Fig. 9 The effect of Deborah number on the normalized maximum attainable neck-in vs. planar to uniaxial extensional viscosity ratio for virtual polymer melts having high (top), medium (middle) and low (bottom) level of uniaxial extensional strain hardening considering that die exit stress state, $-N_2/N_1$, is equal to 1 (left) and 2 (right). Here, symbols and lines represent utilized viscoelastic 1D membrane model and simple approximate solution model (Eq. 31) predictions, respectively.

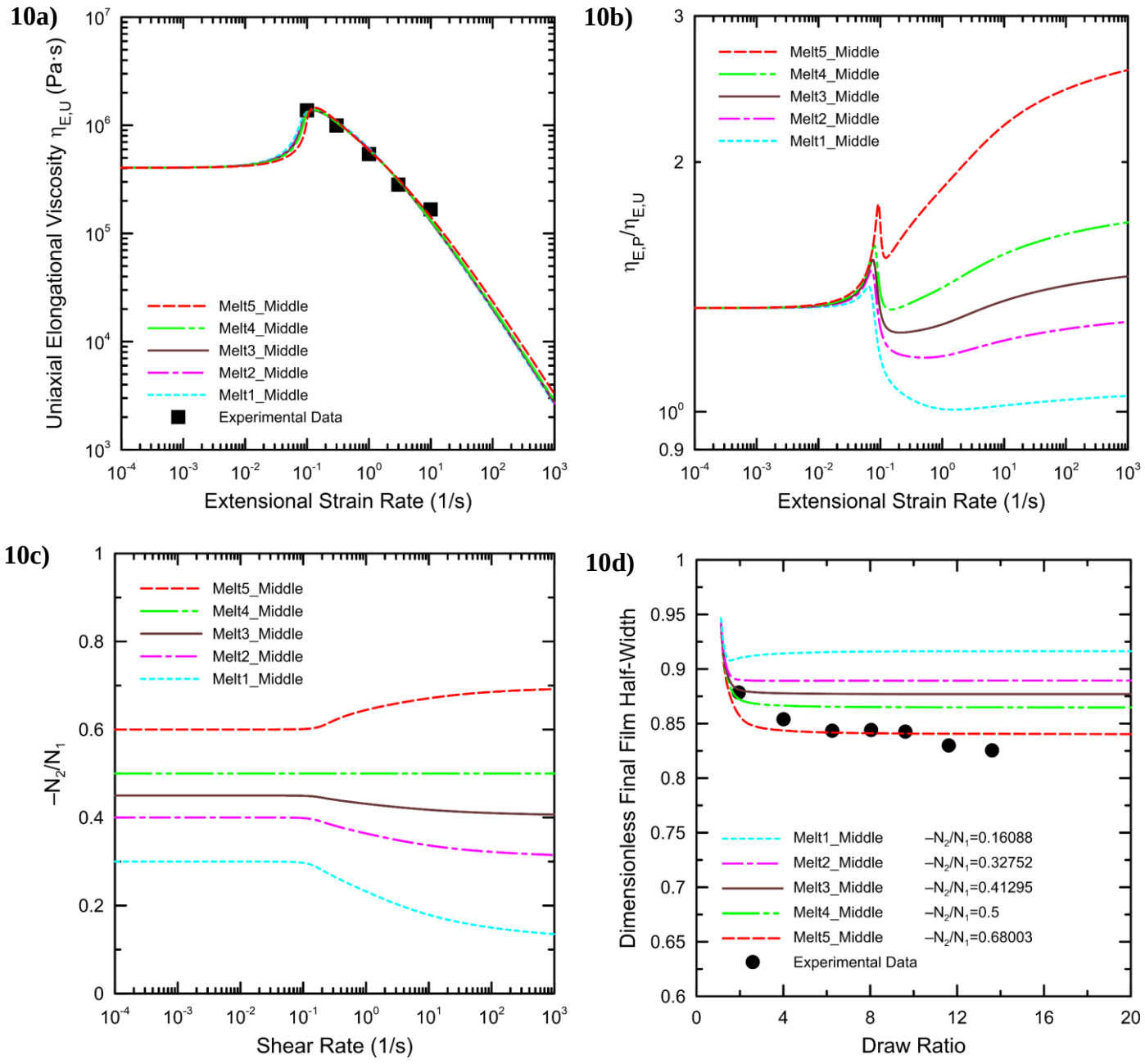

Fig. 10 Comparison between experimental data for LDPE 170A (*T = 150 °C*) and given processing conditions (*De = 0.253*, *X = 10 mm*) taken from [37,38,40] and corresponding model predictions for five virtual materials with modified Leonov model parameters summarized in Table 2. (10a) LDPE 170A uniaxial extensional rheology, (10b) planar to uniaxial extensional viscosity ratio, (10c) second to first normal stress difference ratio, (10d) dimensionless final film half-width as the function of draw ratio.

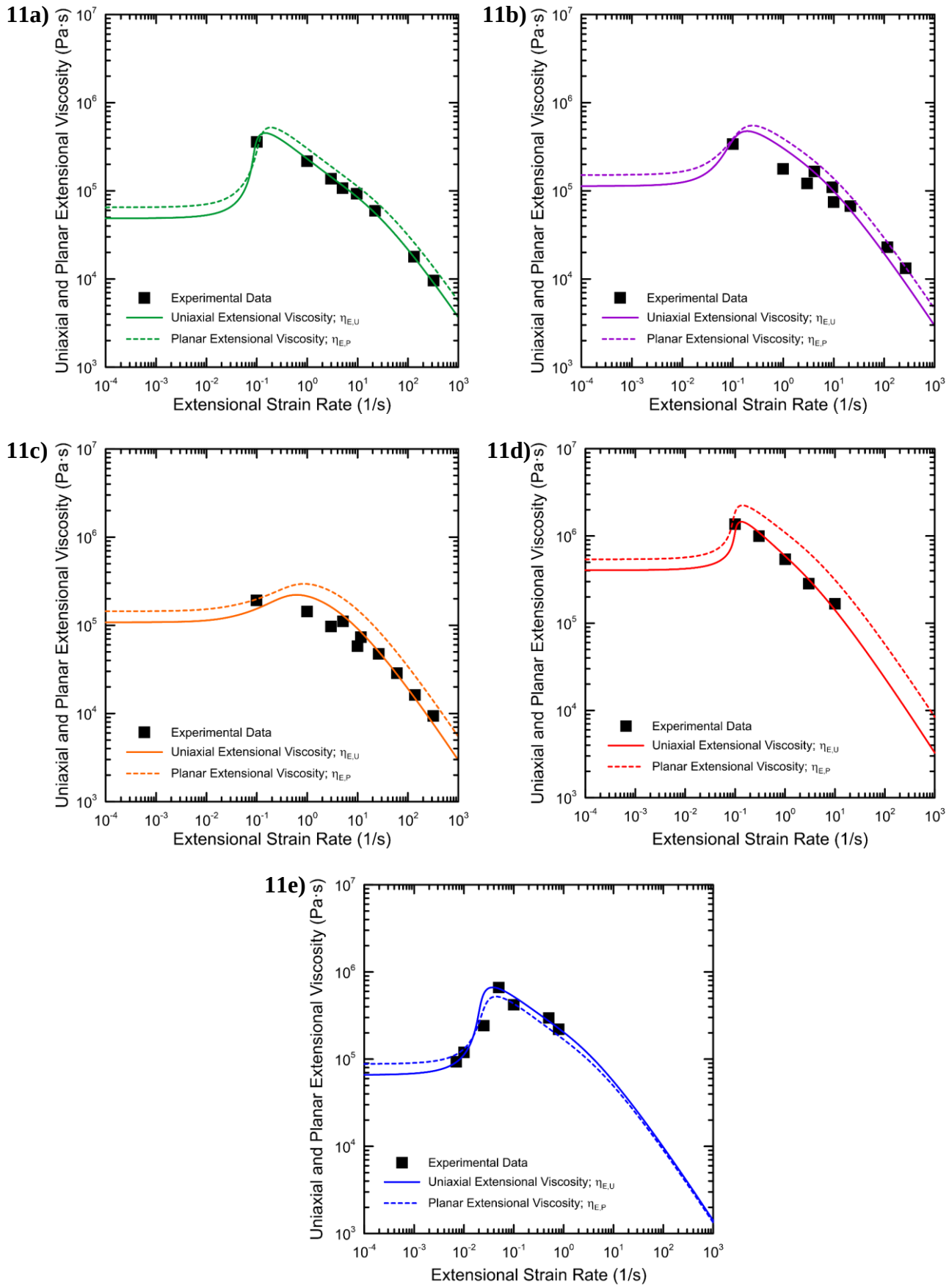

Fig. 11. Comparison between experimental data for deformation rate dependent uniaxial extensional viscosity taken from [47], [37,38,40] and [18], and corresponding single-mode modified Leonov model predictions for uniaxial as well as planar extensional viscosities. (11a) PE-A, *T = 130 °C*, (11b) PE-B, *T = 130 °C*, (11c) PE-C, *T = 130 °C*, (11d) LDPE 170A, *T = 150 °C*, (11e) LDPE C, *T = 125 °C*.

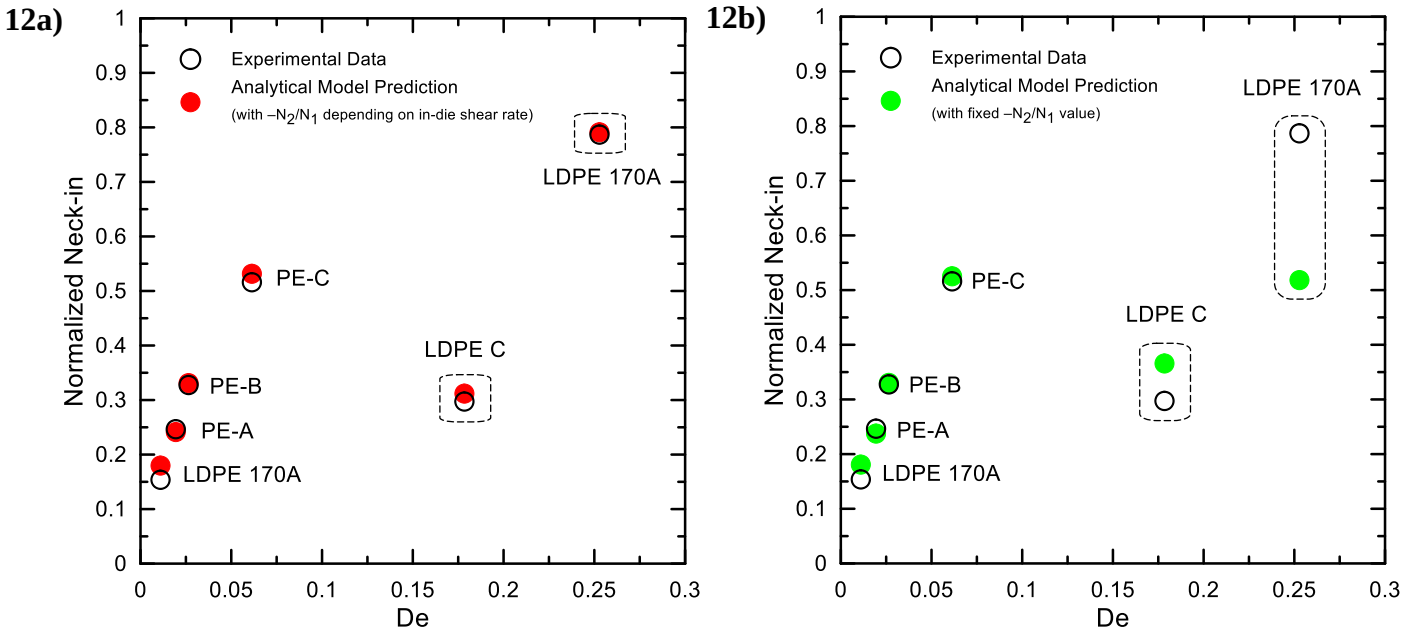

Fig. 12 Normalized maximum attainable neck-in value, NI^*, as the function of Deborah number for LDPE 170A, PE-A, PE-B, PE-C, and LDPE C polymers for the processing conditions summarized in Table 6. Experimental data (taken from [37,38,40], [47] and [18]) and proposed analytical model predictions (Eq. 31) are given here by the open and filled symbols, respectively. (12a) $-N_2/N_1$ is given by the modified Leonov model predictions for particular die exit shear rates, which are provided in Table 7 for each individual case, (12b) $-N_2/N_1$ is considered to be constant, equal to 0.2.